

# Edge Federated Learning Via Unit-Modulus Over-The-Air Computation

Shuai Wang, Yuncong Hong, Rui Wang, Qi Hao, Yik-Chung Wu, and Derrick Wing Kwan Ng

## Abstract

Edge federated learning (FL) is an emerging machine learning paradigm that trains a global parametric model from distributed datasets via wireless communications. This paper proposes a unit-modulus over-the-air computation (UM-AirComp) framework to facilitate efficient edge federated learning, which simultaneously uploads local model parameters and updates global model parameters via analog beamforming. The proposed framework avoids sophisticated baseband signal processing, leading to low communication delays and implementation costs. A training loss bound of UM-AirComp is derived and two low-complexity algorithms, termed penalty alternating minimization (PAM) and accelerated gradient projection (AGP), are proposed to minimize the nonconvex nonsmooth loss bound. Simulation results show that the proposed UM-AirComp framework with PAM algorithm not only achieves a smaller mean square error of model parameters' estimation, training loss, and testing error, but also requires a significantly shorter runtime than that of other benchmark schemes. Moreover, the proposed UM-AirComp framework with AGP algorithm achieves satisfactory performance while reduces the computational complexity by orders of magnitude compared with existing optimization algorithms. Finally, we demonstrate the implementation of UM-AirComp in a vehicle-to-everything autonomous driving simulation platform. It is found that autonomous driving tasks are more sensitive to model parameter errors than other tasks since the former neural networks are more sophisticated containing sparser model parameters.

## Index Terms

Analog beamforming, autonomous driving, federated learning, over-the-air computation, unit-modulus.

Shuai Wang is with the Department of Electrical and Electronic Engineering, the Department of Computer Science and Engineering, and the Sifakis Research Institute of Trustworthy Autonomous Systems, Southern University of Science and Technology (SUSTech), Shenzhen 518055, China (e-mail: wang3@sustech.edu.cn). Yuncong Hong and Rui Wang are with the Department of Electrical and Electronic Engineering, Southern University of Science and Technology (SUSTech), Shenzhen 518055, China (e-mail: hongyc@mail.sustech.edu.cn; wang.r@sustech.edu.cn). Qi Hao is with the Department of Computer Science and Engineering and the Sifakis Research Institute of Trustworthy Autonomous Systems, Southern University of Science and Technology (SUSTech), Shenzhen 518055, China (e-mail: hao.q@sustech.edu.cn). Yik-Chung Wu is with the Department of Electrical and Electronic Engineering, The University of Hong Kong, Hong Kong (e-mail: ycwu@eee.hku.hk). Derrick Wing Kwan Ng is with the School of Electrical Engineering and Telecommunications, the University of New South Wales, Australia (email: w.k.ng@unsw.edu.au).

## I. INTRODUCTION

Deep learning has achieved unprecedented breakthrough in image classification, speech recognition, and object detection due to its ability to efficiently extract intricate nonlinear features from high-dimensional data [1]. Typically, deep learning techniques are deployed at a cloud center, which collects data from distributed users and trains a centralized model via gradient-based back propagation [2]–[5]. However, since the users need to share their local data to the cloud, this paradigm could lead to some potential privacy issues, hindering the development of deep learning in extensive applications such as smart cities and financial systems.

To address the privacy issue, federated learning (FL), which trains individual deep learning models at user terminals, has been proposed by Google Research [6], [7]. In the framework of FL, the locally generated data is locally adopted and not shared to any third party. To leverage the data from other users, local model parameters are uploaded periodically to a server for model aggregation and the aggregated global parameters are then broadcast to the users for further local updates. Therefore, FL achieves distributed training while ensuring data privacy [7].

### A. Edge Federated Learning and Related Work

FL was originally developed for wire-line connected systems [7]. To achieve ubiquitous intelligence, a promising solution is edge FL, e.g., [8]–[11], [13]–[17], where users are connected to an edge server via wireless links. However, the convergence of edge FL may take a long time due to limited capacity of wireless channels during the uplink model aggregation step. To reduce the transmission delay, various edge FL designs have been proposed (summarized in Table I), which are mainly categorized into digital modulation [7]–[11] and analog modulation [13]–[17] methods.

For digital modulation and single-antenna systems, data from different users are multiplexed either in the time or the frequency domain. Current works on delay reduction focus on reducing 1) the number of model aggregation iterations [8], 2) the number of users [9], or 3) the number of bits for representing the gradient of back propagation in each iteration [11]. However, since these strategies involve approximation or simplification of the FL procedure, the performance of learning would be degraded inevitably. Another way to reduce the transmission delay is to adopt multiple-input multiple-output (MIMO) technology for transmission so that data from multiple users are multiplexed concurrently in the spatial domain [12].

TABLE I: A Comparison of Existing and Proposed Schemes.

| Modulation     | Work        | MIMO    | RF Chain | Alg. Complex. | Commun. Delay | Objective Function | AirComp | FL Task          |
|----------------|-------------|---------|----------|---------------|---------------|--------------------|---------|------------------|
| <b>Digital</b> | [7]         | ✗       | +        | +             | +++           | N/A                | ✗       | Classification   |
|                | [8], [9]    | ✗       | +        | +             | ++            | Loss Bound         | ✗       | Classification   |
|                | [11]        | ✗       | +        | +             | ++            | Loss Bound         | ✗       | Classification   |
|                | [12]        | Digital | +++      | +++           | ++            | MSE                | ✗       | ✗                |
| <b>Analog</b>  | [14], [15]  | ✗       | +        | +             | +             | Heuristic          | ✓       | Classification   |
|                | [16]        | Digital | +++      | +++           | +             | MSE                | ✓       | Classification   |
|                | [17]        | Digital | +++      | ++            | +             | Noise Variance     | ✓       | Classification   |
|                | <b>Ours</b> | Analog  | +        | +             | +             | Loss Bound         | ✓       | Object Detection |

The symbol “+” means low, “++” means moderate, “+++” means high.

The symbol “✓” means functionality supported, “✗” means functionality not supported.

On the other hand, the key advantage of analog modulation [13]–[17] over digital modulation arises from the ground-breaking idea of over-the-air computation (AirComp).<sup>1</sup> Specifically, if multiple users upload their local parameters simultaneously, a superimposed signal, which represents a weighted sum of individual model parameters, is observed at the edge server. By performing minimum mean square error (MMSE) detection on the superimposed signal, an estimate of the global parameter vector can be obtained [14], [15]. This significantly saves the transmission time since AirComp in fact exploits inter-user interference in the simultaneous user transmission, in oppose to interference suppression as in digital modulation. However, due to channel fading and noise in wireless systems, AirComp employed in single-antenna systems [14], [15] could result in large error in the estimation of global model parameters at the edge server, leading to slow convergence of FL iterations. As a remedy, adopting MIMO beamforming [16], [17] could reduce the parameter transmission error by aligning the beams carrying the local parameters’ information to the same spatial direction. However, the current transmit and receive beamforming designs in MIMO AirComp systems involve exceedingly high radio frequency (RF) chain costs and high computational complexities [16], [17], preventing their practical implementation.

<sup>1</sup>Recently, it is shown in [18] that digital over-the-air computation can be achieved via exploiting the waveform-superposition property. However, this will introduce additional quantization errors.

In practice, both digital and analog modulation methods share the same goal, i.e., minimizing the training loss function. However, due to the lack of an explicit form of the training loss function with respect to wireless designs, most works focus on other related objective functions such as mean square error (MSE) [16] and noise variance [17]. Recently, the relationship between the training loss function and the wireless designs is derived in [8]–[10]. Nonetheless, the bounds in [8]–[10] are only applicable if the global model parameters are perfectly broadcast to users. For practical cases involving errors in the model broadcast phase, new training loss bounds are required to capture the training performance, which remains an open problem.

### *B. Summary of Challenges and Contributions*

In summary, despite recent exciting development of edge FL techniques, e.g., [7]–[9], [11], [12], [14]–[17], a number of technical challenges remain to be overcome, including

- 1) **Reduction of MIMO implementation costs.** Conventional beamforming designs for base-band signals [12], [16], [17] require one dedicated RF chain per antenna element, which lead to high implementation cost and power consumption. To this end, analog beamforming with a proper phase shift network design [19], [20] can help reduce such implementation costs, which has not been studied in edge FL systems yet.
- 2) **Reduction of beamforming design complexities.** Most beamforming algorithms [12], [16], [17] rely on the execution of the interior point method (IPM). Yet, since IPM involves matrix inversions, these algorithms are with high computational complexities requiring exceedingly long signal processing delay, especially when massive MIMO technique is applied.
- 3) **Verification of robustness in more complex learning tasks.** Existing algorithms in [7]–[9], [11], [12], [14]–[17] are mainly tested on simple image classification tasks (e.g., recognition of handwritten digits). Experiments on more complex and closer-to-reality tasks, such as 3D object detection [21]–[23] in vehicle-to-everything (V2X) autonomous driving systems, are needed to verify the robustness of edge FL.

To fill the research gap, this paper proposes the unit-modulus AirComp (UM-AirComp) framework for edge FL in MIMO communication systems, as shown in Fig. 1. The UM-AirComp framework consists of multiple edge users with local sensing data, one edge server for performing FL, and one communication interface for exchanging model parameters as shown in Fig. 1a. Specifically, the edge users possess a number of training data (e.g., camera images or light detection and ranging (LiDAR) point clouds of the environment with object boundaries or

category labels) for local model training. Then, the trained model parameters are uploaded to the server via analog modulation. To reduce the implementation cost of RF chains, the edge server does not process the received model parameters at the baseband. Instead, it applies a phase shift network (either a fully-connected structure shown in Fig. 1b or a partially-connected structure shown in Fig. 1c) in the RF domain to connect received antennas and transmit antennas for global model updates. Upon receiving the broadcast, all users feed the received signals to an analog demodulator for parameter extraction. The advantages of UM-AirComp and contributions of this paper are summarized below:

- 1) The UM-AirComp at the server significantly reduces the required implementation cost of RF chains in MIMO FL systems, thereby reducing the hardware and energy costs. The training loss of UM-AirComp framework is proved to be upper bounded by a monotonic increasing function of the maximum MSE of the model parameters' estimation. Experimental results confirm the high accuracy of the derived bound.
- 2) Despite the UM-AirComp problem being highly nonconvex, two large-scale optimization algorithms, termed penalty alternating minimization (PAM) and accelerated gradient projection (AGP), are developed for fully-connected UM-AirComp and partially-connected UM-AirComp, respectively. The learning performance of the proposed PAM and AGP is shown to outperform other benchmark schemes. In particular, the AGP algorithm is 100x faster than that of the state-of-the-art second-order optimization algorithms.
- 3) We implement the UM-AirComp edge FL scheme for 3D object detection with multi-vehicle point-cloud datasets in Car Learning to Act (CARLA) simulation platform [24]. To the best of our knowledge, this is the first attempt that edge FL is demonstrated in a V2X auto-driving simulator with a complex deep learning task.

### C. Notation

Italic letters, lowercase and uppercase bold letters represent scalars, vectors, and matrices, respectively. Curlicue letters stand for sets and  $|\cdot|$  is the cardinality of a set. The operators  $\|\cdot\|_2, (\cdot)^T, (\cdot)^H, (\cdot)^{-1}, \lambda_{\max}(\cdot), \lambda_{\min}(\cdot), \text{Null}(\cdot), \text{Rank}(\cdot)$  are the  $\ell_2$ -norm, transpose, Hermitian, inverse, largest eigenvalue, smallest eigenvalue, null space, and rank of a matrix, respectively. The operators  $\partial f$  and  $\nabla f$  are the partial derivative and the gradient of the function  $f$ . The function  $[x]^+ = \max(x, 0)$ ,  $\text{Re}(x)$  takes the real part of  $x$ ,  $\text{Im}(x)$  takes the imaginary part of  $x$ ,  $\text{conj}(x)$  takes the conjugate of  $x$ , and  $|x|$  is the modulus of  $x$ .  $\mathbf{I}_N$  denotes the  $N \times N$  identity

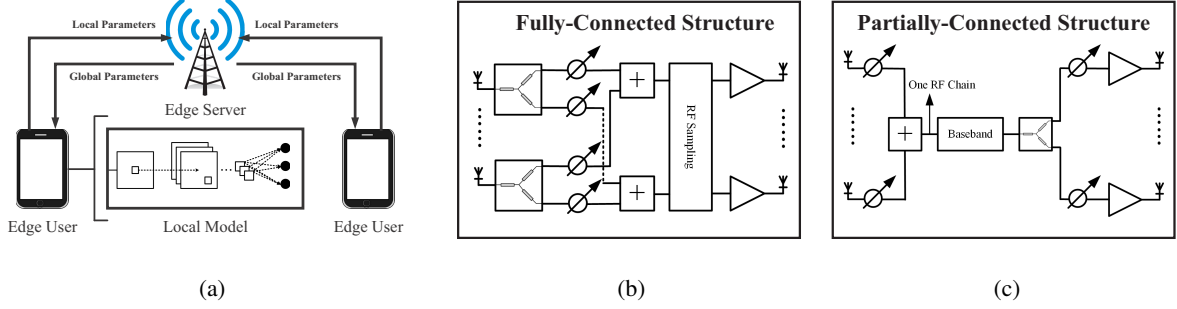


Fig. 1: a) Illustration of an edge FL system; b) fully-connected phase shift network structure; c) partially-connected phase shift network structure.

matrix,  $\mathbf{1}_N$  represents the  $N \times 1$  all-ones vector, and  $\mathbf{A} \succeq \mathbf{B}$  represents  $\mathbf{A} - \mathbf{B}$  being positive semidefinite. Finally,  $j = \sqrt{-1}$ ,  $\mathbb{E}(\cdot)$  denotes the expectation of a random variable and  $\mathcal{O}(\cdot)$  is the big-O notation standing for the order of arithmetic operations.

## II. EDGE FEDERATED LEARNING WITH AIRCOMP

We consider an FL system shown in Fig. 1, which consists of an edge server equipped with  $N$  antennas and  $K$  single-antenna mobile users. The dataset and model parameter vector at user  $k$  are denoted as  $\mathcal{D}_k$  and  $\mathbf{x}_k \in \mathbb{R}^{M \times 1}$ , respectively. Mathematically, the FL procedure aims to solve the following optimization problem:

$$\min_{\{\mathbf{x}_k\}, \boldsymbol{\theta}} \underbrace{\frac{1}{\sum_{k=1}^K |\mathcal{D}_k|} \sum_{k=1}^K \sum_{\mathbf{d}_l \in \mathcal{D}_k} \Theta(\mathbf{d}_l, \boldsymbol{\theta})}_{:=\Lambda(\boldsymbol{\theta})} \quad \text{s.t.} \quad \mathbf{x}_1 = \cdots = \mathbf{x}_K = \boldsymbol{\theta}, \quad (1)$$

where  $\Theta(\mathbf{d}_l, \boldsymbol{\theta})$  is the loss function corresponding to a single sample  $\mathbf{d}_l$  ( $1 \leq l \leq |\mathcal{D}_k|$ ) in  $\mathcal{D}_k$  given parameter vector  $\boldsymbol{\theta}$ , while  $\Lambda(\boldsymbol{\theta})$  denotes the global loss function to be minimized. The training of FL model parameters (i.e., solving (1)) in the considered edge system is naturally a distributed and iterative procedure, where each iteration involves two steps: 1) updating the local parameter vectors  $(\mathbf{x}_1, \dots, \mathbf{x}_K)$  using  $\{\mathcal{D}_1, \dots, \mathcal{D}_K\}$  at users  $(1, \dots, K)$ , respectively; and 2) aggregating  $(\mathbf{x}_1, \dots, \mathbf{x}_K)$  in an analog manner at the edge server and notifying the users. The above two steps are further elaborated below.

In the first step, let  $\mathbf{x}_k^{[i]}(0) \in \mathbb{R}^{M \times 1}$  be the local parameter vector at user  $k$  at the beginning of the  $i$ -th iteration. To update  $\mathbf{x}_k^{[i]}(0)$ , user  $k$  minimizes the loss function  $\frac{1}{|\mathcal{D}_k|} \sum_{\mathbf{d}_l \in \mathcal{D}_k} \Theta(\mathbf{d}_l, \mathbf{x}_k)$

via gradient descent<sup>2</sup> as

$$\mathbf{x}_k^{[i]}(\tau + 1) = \mathbf{x}_k^{[i]}(\tau) - \frac{\varepsilon}{|\mathcal{D}_k|} \sum_{\mathbf{d}_l \in \mathcal{D}_k} \nabla_{\mathbf{x}} \Theta(\mathbf{d}_l, \mathbf{x}) \big|_{\mathbf{x}=\mathbf{x}_k^{[i]}(\tau)}, \quad k = 1, \dots, K, \quad (2)$$

where  $\varepsilon$  is the step-size and  $\tau$  is from 0 to  $E - 1$  with  $E$  being the number of local updates. Then,  $\{\mathbf{x}_k^{[i]}(E) | \forall k\}$  from all users are uploaded to the edge server.

In the second step, uplink model aggregation and downlink broadcast beamforming should be designed. Specifically, at the  $i$ -th iteration, user  $k$  modulates its local parameter vector  $\mathbf{x}_k^{[i]}(E)$  into a complex vector  $\mathbf{s}_k^{[i]} = \Omega_k^{[i]}(\mathbf{x}_k^{[i]}(E)) \in \mathbb{C}^{S \times 1}$ , where  $\Omega_k^{[i]}(\cdot)$  denotes the modulation function and  $S$  is the vector dimension. The received signal  $\mathbf{R}^{[i]} \in \mathbb{C}^{N \times S}$  at the server is

$$\mathbf{R}^{[i]} = \sum_{k=1}^K \mathbf{h}_k^{[i]} (\mathbf{s}_k^{[i]})^T + \mathbf{Z}^{[i]}, \quad (3)$$

where  $\mathbf{h}_k^{[i]} \in \mathbb{C}^{N \times 1}$  is the uplink channel vector from user  $k$  to the server and  $\mathbf{Z}^{[i]} \in \mathbb{C}^{N \times S}$  is the matrix of the additive white Gaussian noise with covariance matrix  $\mathbb{E} [\text{vec}(\mathbf{Z}^{[i]}) \text{vec}(\mathbf{Z}^{[i]})^H] = \sigma_b^2 \mathbf{I}_{NS}$ , where  $\sigma_b^2$  is the noise power at the server. Upon receiving the superimposed signal, the server processes  $\mathbf{R}^{[i]}$  using a function  $\Psi^{[i]}(\cdot)$  and broadcasts  $\Psi^{[i]}(\mathbf{R}^{[i]}) \in \mathbb{C}^{N \times S}$  to all the users. As a result, the received signal at user  $k$  is

$$(\mathbf{y}_k^{[i]})^T = (\mathbf{g}_k^{[i]})^H \Psi^{[i]}(\mathbf{R}^{[i]}) + (\mathbf{n}_k^{[i]})^T, \quad (4)$$

where  $\mathbf{g}_k^{[i]} \in \mathbb{C}^{N \times 1}$  is the downlink channel vector from the server to user  $k$ , and  $\mathbf{n}_k^{[i]} \in \mathbb{C}^{S \times 1}$  is the vector of the additive white Gaussian noise with covariance matrix  $\sigma_k^2 \mathbf{I}_S$ , where  $\sigma_k^2$  is the noise power at user  $k$ . Finally, user  $k$  applies a demodulation function  $\overline{\Omega}_k^{[i]}(\cdot)$  to  $\mathbf{y}_k^{[i]}$  and sets the local parameter vector for the  $(i + 1)$ -th iteration as  $\mathbf{x}_k^{[i+1]}(0) = \overline{\Omega}_k^{[i]}(\mathbf{y}_k^{[i]})$ . Expanding the expression of  $\mathbf{y}_k^{[i]}$  in (4) yields

$$\mathbf{x}_k^{[i+1]}(0) = \overline{\Omega}_k^{[i]} \left( (\mathbf{g}_k^{[i]})^H \Psi^{[i]} \left( \sum_{k=1}^K \mathbf{h}_k^{[i]} \left[ \Omega_k^{[i]}(\mathbf{x}_k^{[i]}(E)) \right]^T + \mathbf{Z}^{[i]} \right) + (\mathbf{n}_k^{[i]})^T \right). \quad (5)$$

Edge FL aims to design  $\{\Omega_k^{[i]}, \overline{\Omega}_k^{[i]}, \Psi^{[i]}\}$  such that  $\mathbb{E} [\|\mathbf{x}_k^{[i+1]}(0) - \boldsymbol{\theta}^{[i]}\|_2^2]$  is minimized, where

$$\boldsymbol{\theta}^{[i]} = \sum_{k=1}^K \frac{|\mathcal{D}_k|}{\sum_{l=1}^K |\mathcal{D}_l|} \mathbf{x}_k^{[i]}(E) \quad (6)$$

is equivalent to the gradient descent of the objective function of (1). In existing AirComp schemes, e.g., [13]–[17],  $\Omega_k^{[i]}$  is implemented using analog modulation,  $\Psi^{[i]}$  is implemented using

<sup>2</sup>If  $|\mathcal{D}_k|$  is large, stochastic gradient descent can be adopted to accelerate the training speed.

a MIMO transceiver, and  $\overline{\Omega}_k^{[i]}$  is implemented using digital demodulation. Thus, the superimposed signals of all receive antennas at the edge server are first combined via a vector in the digital baseband and then broadcast to users via another vector in the baseband. Therefore, the required number of RF chains at the edge server should equal the number of antennas. Note that the associated implementation cost could be high if massive number of antennas are deployed. In the following section, the UM-AirComp scheme, where the functions  $\{\Omega_k^{[i]}, \overline{\Omega}_k^{[i]}, \Psi^{[i]}\}$  are almost implemented in analog domain, is proposed. This helps to reduce both the required implementation costs of RF chains and power consumption while achieving excellent system performance.

### III. PROPOSED UM-AIRCOMP EDGE FL FRAMEWORK

#### A. UM-AirComp Framework

The proposed UM-AirComp scheme consists of: 1) analog modulation designs for local model upload at all users; 2) analog beamforming at the edge server which employs phase shifters (unit-modulus) to generate updated global model parameters from the local ones; 3) analog demodulation designs at all users for global model reconstruction. The three components are detailed as follows.

**1) Structure of analog modulation  $\Omega_k^{[i]}$ .** The deep learning model parameters are transmitted in an analog manner as in [13]–[15]. Specifically, since the model parameters in deep learning are real-valued numbers, in order to reduce the transmission time, every two model parameters are transmitted as a complex number. That is,

$$\mathbf{s}_k^{[i]} = \Omega_k^{[i]} \left( \mathbf{x}_k^{[i]}(E) \right) = \frac{\sqrt{p_k^{[i]}} \exp(j\varphi_k^{[i]})}{\sqrt{2\eta^{[i]}}} \left[ x_{k,1}^{[i]}(E) + j x_{k,2}^{[i]}(E), \dots, x_{k,M-1}^{[i]}(E) + j x_{k,M}^{[i]}(E) \right]^T, \quad (7)$$

where  $\mathbf{s}_k^{[i]} \in \mathbb{C}^{S \times 1}$  with  $S = M/2$  and  $x_{k,m}^{[i]}(E)$  is the  $m$ -th element of  $\mathbf{x}_k^{[i]}(E)$ . The scaling factor  $\eta^{[i]}$  is  $\eta^{[i]} = \frac{1}{K} \sum_{k=1}^K \overline{\eta}_k^{[i]}$  with  $\overline{\eta}_k^{[i]} = \frac{1}{M} \|\mathbf{x}_k^{[i]}(E)\|_2^2$  such that the average power of  $\mathbf{s}_k^{[i]}$  is  $\frac{1}{S} \mathbb{E} \left[ \|\mathbf{s}_k^{[i]}\|_2^2 \right] = p_k^{[i]}$ .<sup>3</sup> The transmit power  $p_k^{[i]} \in \mathbb{R}$  satisfies  $p_k^{[i]} \leq P_0$  with  $P_0$  being the maximum transmit power at each user. The transmit phase  $\varphi_k^{[i]} \in [0, 2\pi]$  is adopted to align the phase of

<sup>3</sup>Each user first sends the value of average energy of model parameters to the server for the computation of  $\eta^{[i]}$ . Then, the server sends  $\eta^{[i]}$  to all users. In practice, the users would adopt  $\eta^{[i-1]}$  from the last iteration, which is a good approximation for the actual  $\eta^{[i]}$  in the current iteration.



user  $k$  with those of other users. To facilitate the subsequent derivations, we define the transmit coefficient  $t_k^{[i]} = \sqrt{p_k^{[i]}} \exp(j\varphi_k^{[i]})$  for all  $(i, k)$  and  $\{p_k^{[i]}, \varphi_k^{[i]}\}$  can be recovered from  $\{t_k^{[i]}\}$ .

**2) Structure of unit-modulus beamforming  $\Psi^{[i]}$ .** The computation function  $\Psi^{[i]}$  adopted at the edge server weighs the amplitude and phase of the signal  $\mathbf{R}^{[i]}$ . We propose to aggregate and forward the signal via

$$\Psi^{[i]}(\mathbf{R}^{[i]}) = \sqrt{\gamma} \mathbf{F}^{[i]} \mathbf{R}^{[i]}, \quad (8)$$

where  $\gamma > 0$  is the power scaling factor at the edge server and  $\mathbf{F}^{[i]} \in \mathbb{C}^{N \times N}$  is the phase shift matrix. The implementation of  $\mathbf{F}^{[i]}$  can be either fully-connected or partially-connected [19], [20]. For the former structure, each receive antenna element is connected to all transmit antenna elements via a network of phase shifters as shown in Fig. 1b. This results in unit-modulus constraints on all elements of the analog beamforming matrices  $\{\mathbf{F}^{[i]}\}$ , i.e.,

$$|F_{l,l'}^{[i]}| = 1, \quad \forall l, l', \quad (9)$$

and the required number of phase shifters is  $N^2$ . For the latter structure, each receive antenna element is combined via a phase shift vector and then connected to transmit antenna elements via another phase shift vector as shown in Fig. 1c. Hence, apart from the unit-modulus constraint (9),  $\mathbf{F}^{[i]}$  should also satisfy  $\text{Rank}(\mathbf{F}^{[i]}) = 1$ . Note that the required number of total phase shifters is only  $2N$ .

**3) Structure of analog demodulation  $\overline{\Omega}_k^{[i]}$ .** The demodulation function  $\overline{\Omega}_k^{[i]}$  maps the received signal  $\mathbf{y}_k^{[i]}$  to  $\mathbf{x}_k^{[i+1]}(0)$ . Since  $\overline{\Omega}_k^{[i]}$  is the reverse operation of  $\{\Omega_k^{[i]}\}$ , the proposed structure for  $\{\overline{\Omega}_k^{[i]}\}$  is written as

$$\mathbf{x}_k^{[i+1]}(0) = \overline{\Omega}_k^{[i]}(\mathbf{y}_k^{[i]}) = \sqrt{2\eta^{[i]}} \left[ \text{Re}(r_k^{[i]} y_{k,1}^{[i]}), \text{Im}(r_k^{[i]} y_{k,1}^{[i]}), \dots, \text{Re}(r_k^{[i]} y_{k,L}^{[i]}), \text{Im}(r_k^{[i]} y_{k,L}^{[i]}) \right]^T, \quad (10)$$

where  $r_k^{[i]} \in \mathbb{C}$  is a normalization coefficient applied to  $\mathbf{y}_k^{[i]}$  and  $y_{k,l}^{[i]}$  is the  $l^{\text{th}}$  element of  $\mathbf{y}_k^{[i]}$ .

*Remark 1 (Duplex Mode):* The proposed UM-AirComp framework can be applied to time division duplex (TDD) systems, where the uplink is separated from the downlink in time by the allocation of different time slots with the same frequency band. For the fully-connected structure, such a time allocation can be implemented via the direct RF sampling technique [25] as shown in Fig. 1b, which achieves significantly lower costs than baseband sampling and computation. For the partially-connected structure, such a time allocation can be implemented at the baseband with only one RF chain, since the phase shifted signals are combined into one stream in the RF domain before down conversion as shown in Fig. 1c.

### B. MSE and Training Loss Analysis

Due to the noise and interference in analog transmission of model parameters, the training loss of  $\Lambda(\mathbf{x}_k^{[i+1]}(0))$  under UM-AirComp scheme would be greater than  $\Lambda(\boldsymbol{\theta}^*)$  in wired FL systems, where  $\boldsymbol{\theta}^*$  denotes the optimal solution of  $\boldsymbol{\theta}$  to (1). Hence, we can use the expectation of their difference, namely  $\mathbb{E} [\Lambda(\mathbf{x}_k^{[i+1]}(0)) - \Lambda(\boldsymbol{\theta}^*)]$ , as a metric to capture the degradation on training loss, which depends on the MSE of the model parameters' estimation. Before establishing the relation between the training loss and MSE, we first derive the expression of MSE and introduce the assumption imposed on loss function. Based on (6) and (10), the MSE between the received local parameter  $\mathbf{x}_k^{[i+1]}$  and the target local parameter  $\boldsymbol{\theta}^{[i]}$  at the  $(i+1)$ -th FL iteration is

$$\begin{aligned} \text{MSE}_k^{[i]} \left( \mathbf{F}^{[i]}, t_k^{[i]}, r_k^{[i]} \right) &= \mathbb{E} \left[ \left\| \mathbf{x}_k^{[i+1]}(0) - \boldsymbol{\theta}^{[i]} \right\|_2^2 \right] \\ &= 2\eta^{[i]} S \left[ \gamma \sum_{j=1}^K \left| r_k^{[i]} (\mathbf{g}_k^{[i]})^H \mathbf{F}^{[i]} \mathbf{h}_j^{[i]} t_j^{[i]} - \alpha_j \right|^2 + \gamma \sigma_b^2 \| r_k^{[i]} (\mathbf{g}_k^{[i]})^H \mathbf{F} \|_2^2 + \sigma_k^2 |r_k^{[i]}|^2 \right], \end{aligned} \quad (11)$$

where  $\alpha_k = \frac{|\mathcal{D}_k|}{\sum_{l=1}^K |\mathcal{D}_l|}$  and the equality is due to (7), (10), and the independence among  $\{\mathbf{s}_k | \forall k\}$ .

**Assumption 1.** (i) The function  $\Lambda(\mathbf{x})$  is  $\mu$ -strongly convex. (ii) The function  $\sum_{\mathbf{d}_l \in \mathcal{D}_k} \Theta(\mathbf{d}_l, \mathbf{x})$  is twice differentiable and satisfies  $\sum_{\mathbf{d}_l \in \mathcal{D}_k} \nabla_{\mathbf{x}}^2 \Theta(\mathbf{d}_l, \mathbf{x}) \preceq L\mathbf{I}$ .

Under Assumption 1, the relationship between  $\Lambda(\mathbf{x}_k^{[i+1]}(0))$  and  $\Lambda(\boldsymbol{\theta}^*)$  is summarized in the following theorem.

**Theorem 1.** With  $(\varepsilon, E) = (\frac{\sum_{k=1}^K |\mathcal{D}_k|}{KL}, 1)$ , the UM-AirComp scheme satisfies

$$\mathbb{E} \left[ \Lambda(\mathbf{x}_k^{[i+1]}(0)) - \Lambda(\boldsymbol{\theta}^*) \right] \leq \sum_{i'=0}^i A^{[i']} \max_{k=1, \dots, K} \text{MSE}_k^{[i']}, \quad (12)$$

for any  $\{\mathbf{F}^{[i']}, r_k^{[i']}, t_k^{[i']}\}_{i'=1}^i$  as  $i \rightarrow +\infty$ , where  $A^{[i']} = \frac{KL(3+2K^{-1})}{2 \sum_{k=1}^K |\mathcal{D}_k|} \left( 1 - \frac{\mu \sum_{k=1}^K |\mathcal{D}_k|}{KL} \right)^{i-i'}$ .

*Proof.* See Appendix A. ■

Theorem 1 shows a diminishing  $A^{[i']} \rightarrow 0$  for a large  $i-i'$ , meaning that the impact from earlier FL iterations vanishes as the edge FL continues. On the other hand, if  $\text{MSE}_k^{[i']} \rightarrow 0$  for all  $k$ , then  $\Lambda(\mathbf{x}_k^{[i+1]})$  is an unbiased estimate of  $\Lambda(\boldsymbol{\theta}^*)$ . This demonstrates the effectiveness of UM-AirComp in the asymptotic region. The convexity and smoothness in Assumption 1 have been adopted in most loss bound analysis of FL (e.g., [26], [40]). Although it seems to be restrictive for realistic applications, analysis under Assumption 1 could provide important insights of the behavior of

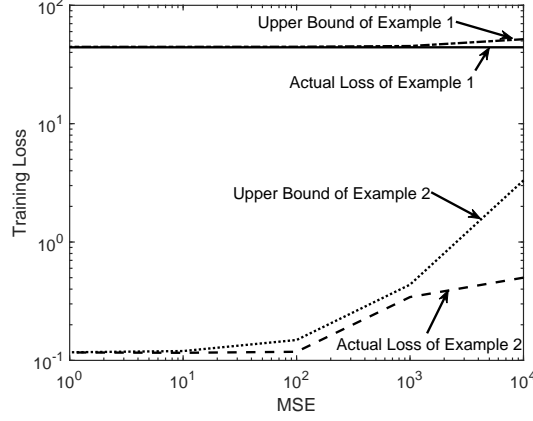


Fig. 2: Comparison between the actual training loss and loss bound at  $\text{MSE}_k^{[i']} = (1, 10, 100, 1000, 10000)$  when  $K = 10$  and  $|\mathcal{D}_k| = 100$  after 1000 FL iterations.

UM-AirComp in nonconvex cases. In particular, a nonconvex function can be locally convex within the neighborhood of the optimal solution  $\theta^*$  of (1). Therefore, if the learning model is pre-trained such that  $\mathbf{x}_k^{[0]}$  is in the neighborhood of  $\theta^*$ , then the analysis based on Assumption 1 is also valid for nonconvex loss functions. On the other hand, if the pre-trained model parameters are not in the neighborhood of  $\theta^*$ , the result can be treated as an approximation of the upper bound with  $L \propto \varepsilon^{-1}$  and  $\mu \propto (\sum_{k=1}^K |\mathcal{D}_k|)^{-1}$ .

To verify the correctness of Theorem 1, the case of  $K = 10$  and  $|\mathcal{D}_k| = 100$  is simulated. Since the result in Theorem 1 is valid for any design of  $\{\mathbf{F}^{[i']}, r_k^{[i']}, t_k^{[i']}\}$ , for the purpose of demonstration, we set  $\text{MSE}_k^{[i']} = (1, 10, 100, 1000, 10000)$  at all users for  $i' = (1, \dots, 1000)$ . Then, we consider the following examples:

- **Example 1: Linear regression.** The dataset  $\mathcal{D}_k$  consists of input-output pairs  $\mathbf{d}_l = (\mathbf{d}_l^{\text{in}}, d_l^{\text{out}})$  to be fitted, where the input vector  $\mathbf{d}_l^{\text{in}} \in \mathbb{R}^{M \times 1}$  is generated from  $\mathbf{d}_l^{\text{in}} \sim \mathcal{N}(\mathbf{0}, 0.0001 \mathbf{I}_{100})$  and the output value  $d_l^{\text{out}} \in \mathbb{R}$  is generated from  $d_l^{\text{out}} \sim \mathcal{N}(\mathbf{1000}^T \mathbf{d}_l^{\text{in}}, 10)$ . The loss function  $\Theta(\mathbf{d}_l, \mathbf{x}_k) = (\mathbf{x}_k^T \mathbf{d}_l^{\text{in}} - d_l^{\text{out}})^2 / 2$ . The parameters  $L$  can be computed as the largest eigenvalue of matrix  $\sum_{\mathbf{d}_l \in \mathcal{D}_k} \mathbf{d}_l \mathbf{d}_l^H$  for all  $k$  and  $\mu$  can be computed as the smallest eigenvalue of matrix  $(\sum_{k=1}^K |\mathcal{D}_k|)^{-1} \sum_{\mathbf{d}_l \in \{\mathcal{D}_1, \dots, \mathcal{D}_K\}} \mathbf{d}_l \mathbf{d}_l^H$ . The training step-size is set to  $\varepsilon = 1/L$ .
- **Example 2: Image classification via a convolutional neural network (CNN).** The mixed national institute of standards and technology (MNIST) dataset is used, where  $\mathbf{d}_l^{\text{in}} \in \mathbb{R}^{784 \times 1}$  is a gray-scale vector of images and  $\mathbf{d}_l^{\text{out}} \in \mathbb{R}^{10 \times 1}$  is a label vector containing only one non-zero element. The CNN consists of two convolution layers, two max pooling layers, and a

fully-connected layer. Denoting  $f_{\text{cnn}}(\mathbf{x}_k, \mathbf{d}_l^{\text{in}})$  as the softmax output of CNN given parameter vector  $\mathbf{x}_k$  and the input vector  $\mathbf{d}_l^{\text{in}}$ , the loss function  $\Theta(\mathbf{d}_l, \mathbf{x}_k) = [f_{\text{cnn}}(\mathbf{x}_k, \mathbf{d}_l^{\text{in}}) - \mathbf{d}_l^{\text{out}}]^2 / 2$ . The training step-size is set to  $\varepsilon = 1$ . The parameter  $L$  and  $\mu$  are set to  $L = 0.1 \varepsilon / K$  and  $\mu = 0.5 (\sum_{k=1}^K |\mathcal{D}_k|)^{-1}$ .

It can be seen from Fig. 2 that the training loss after 1000 FL iterations is indeed upper bounded by the expression derived in Theorem 1. Moreover, the bound is tight for Example 1 due to its convex loss function, while it is slightly looser for Example 2 due to its nonconvex loss function. Note that no matter which task is considered, the upper bound derived in Theorem 1 matches the trend of the actual loss very well.

### C. Problem Formulation

Ideally, the optimization of  $\{\mathbf{F}^{[i]}, r_k^{[i]}, t_k^{[i]}\}$  should be performed to minimize the training error, i.e.,  $\min \Lambda(\mathbf{x}_k^{[i+1]}(0))$ . However, the analytical expression of  $\mathbb{E} [\Lambda(\mathbf{x}_k^{[i+1]}(0))]$ , where the expectation is taken over receiver noises and model parameters, is usually challenging to derive. As a compromise approach, we aim to minimize its upper bound  $\Lambda(\boldsymbol{\theta}^*) + \sum_{i'=0}^i A^{[i']} \max_k \text{MSE}_k^{[i']}$  obtained from Theorem 1. Thus, the minimization of training loss in edge FL is formulated as

$$\min_{\{\mathbf{F}^{[i']}, r_k^{[i']}, t_k^{[i']}\}} \sum_{i'=0}^i A^{[i']} \max_{k=1, \dots, K} \text{MSE}_k^{[i']} \left( \mathbf{F}^{[i']}, r_k^{[i']}, t_k^{[i']} \right) \quad (13a)$$

$$\text{s.t.} \quad \mathbf{F}^{[i']} \in \mathcal{F}, \quad i' = 0, \dots, i, \quad (13b)$$

$$|t_k^{[i']}|^2 \leq P_0, \quad k = 1, \dots, K, \quad i' = 0, \dots, i. \quad (13c)$$

The constraint (13b) is the beamforming constraints at the server, with the feasible set

$$\mathcal{F} = \begin{cases} \{\mathbf{F} : |F_{l,l'}| = 1, \forall l, l'\}, & \text{Fully connected} \\ \{\mathbf{F} : \text{Rank}(\mathbf{F}) = 1, |F_{l,l'}| = 1, \forall l, l'\}, & \text{Partially connected} \end{cases}. \quad (14)$$

The constraint (13c) is the power constraints at users obtained from  $|t_k|^2 \leq P_0$ . It can be seen that the above problem and constraints can be decoupled for each iteration and the minimization at the  $i$ -th FL iteration,  $\forall i$ , is given by

$$\mathcal{P} : \min_{\mathbf{F}, \{r_k, t_k\}} \max_{k=1, \dots, K} \underbrace{\left[ \gamma \sum_{j=1}^K \left| r_k \mathbf{g}_k^H \mathbf{F} \mathbf{h}_j t_j - \alpha_j \right|^2 + \gamma \sigma_b^2 \|r_k (\mathbf{g}_k)^H \mathbf{F}\|_2^2 + \sigma_k^2 |r_k|^2 \right]}_{\text{MSE}_k / (2\eta S)} \quad (15a)$$

$$\text{s.t.} \quad \mathbf{F} \in \mathcal{F}, \quad (15b)$$

$$|t_k|^2 \leq P_0, \quad k = 1, \dots, K, \quad (15c)$$

where the FL iteration index  $i'$  and  $A^{[i']}$  are omitted. This is because  $A^{[i']}$  is a constant given the tuple of system parameters  $(K, \sum_k |\mathcal{D}_k|, \mu, L)$  in a particular FL iteration. The term  $\text{MSE}_k/(2\eta S)$  is the normalized MSE with respect to the power of each parameter. It can be seen that the key to minimize the training loss upper bound of UM-AirComp is to minimize the *maximum MSE* instead of the average MSE.

*Remark 2 (Challenges of Solving  $\mathcal{P}$ ):* Problem  $\mathcal{P}$  is NP-hard due to the unit-modulus constraints [19], [20]. In addition, the coupling between variables  $\{r_k\}$ ,  $\{t_k\}$ , and  $\mathbf{F}$  makes the problem nonlinear and nonconvex. Furthermore, the large dimensions of  $\mathbf{F}$  and  $\{r_k, t_k\}$  call for the design of low-complexity algorithms in the scenario with massive numbers of antennas and users.

#### IV. PENALTY ALTERNATING MINIMIZATION FOR FULLY-CONNECTED UM-AIRCOMP

In this section, the UM-AirComp with fully-connected structure is studied, where the feasible set  $\mathcal{F}$  is given in the first line of (14). A PAM algorithm with two layers of iterations, i.e., an outer-layer iteration and an inner-layer iteration, will be proposed to optimize the system performance. Below we first introduce the outer-layer iteration.

##### A. Outer-Layer Iteration

To resolve the coupling between variables  $\{r_k\}$ ,  $\{t_k\}$ , and  $\mathbf{F}$ , this paper adopts an alternating optimization framework [28], which optimizes one design variable at a time with others being fixed. Starting with an initial solution  $\{\mathbf{F}^{(0)}, r_k^{(0)}, t_k^{(0)}\}$ , the entire procedure solving the problem  $\mathcal{P}$  for the  $(n+1)$ -th outer iteration,  $\forall n$ , can be elaborated below:

$$\begin{aligned} \mathbf{F}^{(n+1)} = \arg \min_{\mathbf{F}} \max_{k=1, \dots, K} & \left( \sum_{j=1}^K \left| r_k^{(n)} \mathbf{g}_k^H \mathbf{F} \mathbf{h}_j t_j^{(n)} - \alpha_j \right|^2 + \sigma_b^2 \| r_k^{(n)} \mathbf{g}_k^H \mathbf{F} \|_2^2 \right) \\ \text{s.t. } & |F_{l,l'}| = 1, \quad l = 1, \dots, N, \quad l' = 1, \dots, N, \end{aligned} \quad (16a)$$

$$\begin{aligned} \{r_k^{(n+1)}\} = \arg \min_{\{r_k\}} \max_{k=1, \dots, K} & \left( \gamma \sum_{j=1}^K \left| r_k \mathbf{g}_k^H \mathbf{F}^{(n+1)} \mathbf{h}_j t_j^{(n)} - \alpha_j \right|^2 + \gamma \sigma_b^2 \| r_k \mathbf{g}_k^H \mathbf{F}^{(n+1)} \|_2^2 + \sigma_k^2 |r_k|^2 \right), \end{aligned} \quad (16b)$$

$$\{t_k^{(n+1)}\} = \arg \min_{\{t_k\}} \max_{k=1, \dots, K} \sum_{j=1}^K \left| r_k^{(n+1)} \mathbf{g}_k^H \mathbf{F}^{(n+1)} \mathbf{h}_j t_j - \alpha_j \right|^2$$

$$\text{s.t. } |t_k|^2 \leq P_0, \quad k = 1, \dots, K, \quad (16c)$$

where  $\{\mathbf{F}^{(n)}, t_k^{(n)}, r_k^{(n)}\}$  is the solution at the  $n$ -th outer iteration. The iterative procedure stops until  $n$  reaches the maximum iteration number  $n = N_{\max}$ .

Problem (16a) can be transferred to a convex problem via semidefinite relaxation (SDR) while problems (16b) and (16c) are convex. Hence, problems (16a)–(16c) can all be solved via CVX, a Matlab software package for solving convex problems based on interior point method (IPM). According to [30], the computational complexity is at least  $\mathcal{O}(N^7)$  for solving (16a) (the vectorization of  $\mathbf{F}$  involves  $N^2$  variables) and  $\mathcal{O}(K^{3.5})$  for solving (16b)–(16c). For large  $N$  and  $K$ , this method is not desirable. In the following, a new algorithm termed PAM, which decomposes (16a)–(16c) into smaller subproblems that are either solved by gradient updates or closed-form updates, is proposed for achieving both excellent performance and significantly lower computational complexities.

### B. Inner-Layer Iteration

1) *Optimization of  $\mathbf{F}$* : Since  $\mathbf{F}$  is a matrix, its vectorization is given as  $\mathbf{f} = \text{vec}(\mathbf{F}) \in \mathbb{C}^{N^2 \times 1}$ . Applying  $\text{Tr}(\mathbf{AXBX}^T) = \text{vec}(\mathbf{X})^T (\mathbf{B}^T \otimes \mathbf{A}) \text{vec}(\mathbf{X})$  [27], we have

$$r_k^{(n)} \mathbf{g}_k^H \mathbf{F} \mathbf{h}_j t_j^{(n)} = r_k^{(n)} t_j^{(n)} (\mathbf{h}_j^T \otimes \mathbf{g}_k^H) \text{vec}(\mathbf{F}) = (\mathbf{a}_{k,j}^{(n)})^H \mathbf{f}, \quad (17)$$

$$\sigma_b^2 \|r_k^{(n)} \mathbf{g}_k^H \mathbf{F}\|_2^2 = |r_k^{(n)}|^2 \text{Tr}(\mathbf{g}_k \mathbf{g}_k^H \mathbf{F} \mathbf{I}_N \mathbf{F}^H) = \mathbf{f}^H \mathbf{G}_k^{(n)} \mathbf{f}, \quad (18)$$

where  $\mathbf{G}_k^{(n)} = \sigma_b^2 |r_k^{(n)}|^2 \mathbf{I}_N \otimes (\mathbf{g}_k \mathbf{g}_k^H)$  and  $\mathbf{a}_{k,j}^{(n)} = [r_k^{(n)} t_j^{(n)} (\mathbf{h}_j^T \otimes \mathbf{g}_k^H)]^H$ . Problem (16a) is thus re-formulated as

$$\begin{aligned} \mathcal{P}_F : \min_{\mathbf{f}} \quad & \max_{k=1, \dots, K} \left( \sum_{j=1}^K \left| (\mathbf{a}_{k,j}^{(n)})^H \mathbf{f} - \alpha_j \right|^2 + \mathbf{f}^H \mathbf{G}_k^{(n)} \mathbf{f} \right) \\ \text{s.t.} \quad & |f_l| = 1, \quad l = 1, \dots, N^2. \end{aligned} \quad (19)$$

To handle the nonseparable objective function, variable splitting of  $\mathbf{f}$  is proposed such that  $\mathbf{f} = \mathbf{u}_1 = \dots = \mathbf{u}_K$ , where  $\{\mathbf{u}_k\}$  are auxilliary variables. Moreover, to handle the unit-modulus constraints, another auxilliary variable  $\mathbf{z} = \mathbf{f}$  is introduced. For all the newly introduced equality constraints, they can be transformed into quadratic penalties in the objective function [29]. As a result,  $\mathcal{P}_F$  is approximately transformed into

$$\min_{\mathbf{f}, \mathbf{z}, \{\mathbf{u}_k\}} \max_{k=1, \dots, K} \left( \sum_{j=1}^K \left| (\mathbf{a}_{k,j}^{(n)})^H \mathbf{u}_k - \alpha_j \right|^2 + \mathbf{u}_k^H \mathbf{G}_k^{(n)} \mathbf{u}_k \right) + \rho \left( \frac{1}{K} \sum_{j=1}^K \|\mathbf{u}_j - \mathbf{f}\|_2^2 + \|\mathbf{z} - \mathbf{f}\|_2^2 \right)$$

$$\text{s.t. } |z_l| = 1, \quad l = 1, \dots, N^2, \quad (20)$$

where  $\rho$  is a tuning parameter. It can be proved that  $\mathcal{P}_F$  and (20) are equivalent problems as  $\rho \rightarrow +\infty$  [29]. However, this case also leads to the gradient norm of the objective function of (20) being infinite, making (20) difficult to solve. Therefore,  $\rho$  controls the tradeoff between approximation error and difficulty in solving (20).

We address (20) using alternating minimization, in which the cost function is iteratively minimized with respect to one variable whereas the others are fixed. Starting with an initial  $\mathbf{f}^{(0)} = \mathbf{z}^{(0)} = \mathbf{u}_{k,j}^{(0)} = \text{vec}(\mathbf{F}^{(n)})$ , the whole process consists of iteratively solving

$$\mathbf{u}_k^{(m+1)} = \arg \min_{\mathbf{u}_k} \sum_{j=1}^K \left| (\mathbf{a}_{k,j}^{(n)})^H \mathbf{u}_k - \alpha_j \right|^2 + \mathbf{u}_k^H \mathbf{G}_k^{(n)} \mathbf{u}_k + \frac{\rho}{K} \|\mathbf{u}_k - \mathbf{f}^{(m)}\|_2^2, \quad \forall k, \quad (21a)$$

$$\mathbf{f}^{(m+1)} = \arg \min_{\mathbf{f}} \rho \left( \frac{1}{K} \sum_{j=1}^K \|\mathbf{u}_j^{(m+1)} - \mathbf{f}\|_2^2 + \|\mathbf{z}^{(m)} - \mathbf{f}\|_2^2 \right), \quad (21b)$$

$$\mathbf{z}^{(m+1)} = \arg \min_{|z_l|=1, \forall l} \rho \|\mathbf{z} - \mathbf{f}^{(m+1)}\|_2^2, \quad (21c)$$

where  $m$  is the inner iteration index. It can be verified that the objective function of (20) is strongly convex. Therefore, despite the non-differentiability of the objective, the alternating minimization (21a)–(21c) is guaranteed to converge to a stationary point of (20) [28]. The iterative procedure stops until  $m$  reaches the maximum iteration number  $m = M_{\max}$ .

The remaining question is how to solve (21a)–(21c) optimally. We notice that problems (21a) and (21b) are standard least squares problems, thus their solutions are given by the following closed-form expressions

$$\mathbf{u}_k^{(m+1)} = \left( \sum_{j=1}^K \mathbf{a}_{k,j}^{(n)} (\mathbf{a}_{k,j}^{(n)})^H + \mathbf{G}_k^{(n)} + \rho \mathbf{I} \right)^{-1} \left( \sum_{j=1}^K \alpha_j \mathbf{a}_{k,j}^{(n)} + \frac{\rho}{K} \mathbf{f}^{(m)} \right), \quad (22)$$

$$\mathbf{f}^{(m+1)} = \frac{1}{2} \left( \frac{1}{K} \sum_{j=1}^K \mathbf{u}_j^{(m+1)} + \mathbf{z}^{(m)} \right), \quad (23)$$

respectively. On the other hand, problem (21c) is the projection of  $\mathbf{f}^{(m+1)}$  onto unit-modulus constraint and the optimal solution is simply

$$\mathbf{z}^{(m+1)} = \exp(j \angle \mathbf{f}^{(m+1)}). \quad (24)$$

2) *Optimization of  $\{r_k\}$* : The problem of optimizing  $\{r_k\}$  in (16b) is also a least squares problem. The optimal solution is found by setting the derivative  $\partial \text{MSE}_k / \partial \text{conj}(r_k)$  to zero:

$$\begin{aligned} \frac{\partial \text{MSE}_k}{\partial \text{conj}(r_k)} &= \gamma \sum_{j=1}^K \left( r_k \mathbf{g}_k^H \mathbf{F}^{(n+1)} \mathbf{h}_j t_j^{(n)} - \alpha_j \right) \text{conj} \left( \mathbf{g}_k^H \mathbf{F}^{(n+1)} \mathbf{h}_j t_j^{(n)} \right) \\ &\quad + \gamma \sigma_b^2 \|\mathbf{g}_k^H \mathbf{F}^{(n+1)}\|_2^2 r_k + \sigma_k^2 r_k = 0 \end{aligned} \quad (25)$$

which yields

$$r_k^{(n+1)} = \frac{\sum_{j=1}^K \alpha_j \text{conj} \left( \mathbf{g}_k^H \mathbf{F}^{(n+1)} \mathbf{h}_j t_j^{(n)} \right)}{\sum_{j=1}^K |\mathbf{g}_k^H \mathbf{F}^{(n+1)} \mathbf{h}_j t_j^{(n)}|^2 + \sigma_b^2 \|\mathbf{g}_k^H \mathbf{F}^{(n+1)}\|_2^2 + \sigma_k^2 / \gamma}. \quad (26)$$

3) *Optimization of  $\{t_k\}$* : The objective function of problem (16c) is not separable. Following similar variable splitting procedure as in (20), we introduce auxiliary variables  $\{\xi_{k,j} = t_k, \forall k, j\}$  and add quadratic penalty  $\rho \sum_{k=1}^K \sum_{j=1}^K |\xi_{k,j} - t_k|^2$  to the objective function. The problem (16c) is approximately transformed into

$$\begin{aligned} \mathcal{P}_t : \min_{\{t_k, \xi_{k,j}\}} \quad & \rho \sum_{k=1}^K \sum_{j=1}^K |\xi_{k,j} - t_j|^2 + \max_{k=1, \dots, K} \sum_{j=1}^K \left| r_k^{(n+1)} \mathbf{g}_k^H \mathbf{F}^{(n+1)} \mathbf{h}_j \xi_{k,j} - \alpha_j \right|^2 \\ \text{s.t.} \quad & |t_k|^2 \leq P_0, \quad k = 1, \dots, K, \end{aligned} \quad (27)$$

and variables  $t_k$  and  $\xi_{k,j}$  can be optimized iteratively. In particular, starting from  $t_k^{(0)} = \xi_{k,j}^{(0)} = t_k^{(n)}$ , the solution of (27) can be obtained iteratively, and the  $q$ -th iteration is given by

$$\xi_{k,j}^{(q+1)} = \arg \min_{\xi_{k,j}} \left| r_k^{(n+1)} \mathbf{g}_k^H \mathbf{F}^{(n+1)} \mathbf{h}_j \xi_{k,j} - \alpha_j \right|^2 + \rho |\xi_{k,j} - t_j^{(q)}|^2, \quad \forall k, j, \quad (28)$$

$$t_j^{(q+1)} = \arg \min_{|t_j|^2 \leq P_0} \rho \sum_{k=1}^K |\xi_{k,j}^{(q+1)} - t_j|^2, \quad \forall j. \quad (29)$$

Problem (28) is a least squares problem and (29) is a quadratic problem with only one constraint. They can be solved optimally based on Karush-Kuhn-Tucker (KKT) conditions and the solutions are given by

$$\xi_{k,j}^{(q+1)} = \frac{\text{conj}(r_k^{(n+1)} \mathbf{g}_k^H \mathbf{F}^{(n+1)} \mathbf{h}_j) \alpha_j + \rho t_j^{(q)}}{|r_k^{(n+1)} \mathbf{g}_k^H \mathbf{F}^{(n+1)} \mathbf{h}_j|^2 + \rho}, \quad \forall k, j, \quad (30)$$

$$t_j^{(q+1)} = \sqrt{\min(P_0, 1)} \frac{\frac{1}{K} \sum_{k=1}^K \xi_{k,j}^{(q+1)}}{\left| \frac{1}{K} \sum_{k=1}^K \xi_{k,j}^{(q+1)} \right|}, \quad \forall j. \quad (31)$$



### C. Summary and Complexity Analysis of PAM

In summary, the complete PAM algorithm for solving problem  $\mathcal{P}$  with a fully-connected structure consists of two layers of iterations. Let  $N_{\max}$  and  $M_{\max}$  denote maximum number of iterations for outer and inner layers. In the outer layer, the PAM optimizes  $\mathbf{F}$ ,  $\{r_k\}$  and  $\{t_k\}$  alternatively in each of the  $N_{\max}$  iterations. In the inner layer,  $\mathbf{F}$  is obtained via computing (22)–(24) for  $M_{\max}$  iterations,  $\{r_k\}$  is obtained via computing (26), and  $\{t_k\}$  is obtained via computing (30)–(31) for  $M_{\max}$  iterations. The computational complexities for these equations are  $\mathcal{O}(KN^2)$ ,  $\mathcal{O}(KN^2)$ ,  $\mathcal{O}(N^2)$ ,  $\mathcal{O}(KN^2)$ ,  $\mathcal{O}(K^2)$ ,  $\mathcal{O}(K^2)$  for (22), (23), (24), (26), (30), (31), respectively. Since the computation is dominant by (22)–(24) with a complexity of  $\mathcal{O}(KN^2)$ , the total computational complexity of PAM is  $\mathcal{O}(N_{\max}M_{\max}KN^2)$ .

### V. ACCELERATED GRADIENT PROJECTION FOR PARTIALLY-CONNECTED UM-AIRCOMP

In practice, it is possible that there are a large number of antennas at the edge server. In such a case, a smaller number of phase shifters than  $N^2$  at the edge server is desirable. To this end, this section proposes an accelerated gradient projection method for partially-connected UM-AirComp, which only needs  $2N$  phase shifters.

With a partially-connected structure as illustrated in Fig. 1c, the feasible set  $\mathcal{F}$  equals the second line of (14). Since the rank of  $\mathbf{F}$  is 1, we can apply rank-one decomposition on  $\mathbf{F}$  which yields  $\mathbf{F} = \mathbf{v}\mathbf{w}^H$ . Then, we adopt the following approximations to  $\mathcal{P}$ : 1) Set  $r_k = 1/(\mathbf{g}_k^H \mathbf{v})$  and  $t_k = 1/(\mathbf{h}_k^H \mathbf{w})$ ; 2) Replace  $\{|F_{l,m}| = 1 \forall l, m\}$  by  $\|\mathbf{F}\|_2^2 \leq N^2$ . After the above steps, problem  $\mathcal{P}$  is simplified into a bilevel form:

$$\mathcal{Q} : \min_{\mathbf{v}} \max_{k=1, \dots, K} \frac{\sigma_k^2}{|\mathbf{g}_k^H \mathbf{v}|^2} \quad \text{s.t.} \quad \frac{N^2}{\|\mathbf{v}\|_2^2} \geq \min_{\mathbf{w}} \left\{ \|\mathbf{w}\|_2^2 : |\mathbf{w}^H \mathbf{h}_k|^2 \geq \frac{\alpha_k^2}{P_0}, \quad \forall k \right\}. \quad (32)$$

Since the right hand side of the constraint in (32) is a quadratic optimization problem, it can be solved by the accelerated random coordinate descent method with a complexity of  $\mathcal{O}(KN)$  [33]. Denoting the solution of  $\mathbf{w}$  using accelerated random coordinate descent method as  $\mathbf{w} = \mathbf{w}^\diamond$ , problem  $\mathcal{Q}$  is reduced to

$$\mathcal{Q}_1 : \min_{\mathbf{v}} \max_{k=1, \dots, K} \frac{\sigma_k^2}{|\mathbf{g}_k^H \mathbf{v}|^2} \quad \text{s.t.} \quad \|\mathbf{v}\|_2^2 \leq \beta, \quad (33)$$

where  $\beta = \frac{N^2}{\|\mathbf{w}^\diamond\|_2^2}$ . In the following, we shall propose an efficient fixed point method for solving problem  $\mathcal{Q}_1$ .

### A. Fixed-Point Iteration

The major challenge in solving problem  $\mathcal{Q}_1$  is the large dimension of variables and the large number of elements inside the maximum operator. To this end, we first re-write  $\mathcal{Q}_1$  as a bilevel problem

$$\min_{\|\mathbf{v}\|_2^2 \leq \beta} \max_{k=1, \dots, K} \frac{\sigma_k^2}{|\mathbf{g}_k^H \mathbf{v}|^2} \iff \min_{\|\mathbf{v}\|_2^2 \leq \beta} \max_{k=1, \dots, K} -\frac{|\mathbf{g}_k^H \mathbf{v}|^2}{\sigma_k^2} \iff \min_{\|\mathbf{v}\|_2^2 \leq \beta} \max_{\mathbf{b} \in \Delta} \underbrace{-\sum_{k=1}^K \frac{b_k |\mathbf{g}_k^H \mathbf{v}|^2}{\sigma_k^2}}_{:=h(\mathbf{v}, \mathbf{b})}, \quad (34)$$

where  $\Delta = \{\mathbf{b} | \mathbf{b} \succeq \mathbf{0}, \mathbf{1}^T \mathbf{b} = 1\}$  and the last step is used to smooth the objective function via introducing one more auxiliary optimization variable  $\mathbf{b}$  [36]. Then, we have the following conclusion on the Karush-Kuhn-Tucker solution to (34), which also holds for  $\mathcal{Q}_1$ .

**Lemma 1.** *Let*

$$U(\mathbf{v}') = \frac{\sqrt{\beta} \mathbf{C}(\mathbf{v}') \arg \min_{\mathbf{b} \in \Delta} \Phi(\mathbf{v}', \mathbf{b})}{\|\mathbf{C}(\mathbf{v}') \arg \min_{\mathbf{b} \in \Delta} \Phi(\mathbf{v}', \mathbf{b})\|_2}, \quad (35)$$

where

$$\Phi(\mathbf{v}', \mathbf{b}) = 2\sqrt{\beta} \|\mathbf{C}(\mathbf{v}') \mathbf{b}\|_2 - [\mathbf{q}(\mathbf{v}')]^T \mathbf{b}, \quad (36)$$

$$\mathbf{C}(\mathbf{v}') = \left[ \frac{\mathbf{g}_1 \mathbf{g}_1^H \mathbf{v}'}{\sigma_1^2}, \dots, \frac{\mathbf{g}_K \mathbf{g}_K^H \mathbf{v}'}{\sigma_K^2} \right] \in \mathbb{C}^{N \times K}, \quad (37)$$

$$\mathbf{q}(\mathbf{v}') = \left[ \frac{|\mathbf{g}_1^H \mathbf{v}'|^2}{\sigma_1^2}, \dots, \frac{|\mathbf{g}_K^H \mathbf{v}'|^2}{\sigma_K^2} \right]^T \in \mathbb{C}^{K \times 1}. \quad (38)$$

Then with any feasible  $\mathbf{v}^{(0)}$  and fixed point iteration  $\mathbf{v}^{(n+1)} \leftarrow U(\mathbf{v}^{(n)})$ , every limit point  $\mathbf{v}^\diamond$  of the sequence  $\{\mathbf{v}^{(0)}, \mathbf{v}^{(1)}, \dots\}$  is a Karush-Kuhn-Tucker solution to problem (34).

*Proof.* See Appendix B. ■

Although Lemma 1 reveals the solution structure of (34), computation of  $U(\mathbf{v}')$  is not straightforward as it involves another optimization problem of  $\mathbf{b}$ , which should also be solved with low computation costs. In the following, we will solve the optimization problem of  $\mathbf{b}$  via the methods of smoothing and acceleration.

### B. Optimization of $\mathbf{b}$ via Smoothing and Acceleration

In order to compute  $U(\mathbf{v}')$ , a necessary step is to find the optimal vector

$$\mathbf{b}^* = \arg \min_{\mathbf{b} \in \Delta} \Phi(\mathbf{b}), \quad (39)$$

where we have omitted the symbol  $\mathbf{v}'$  in (36) since  $\mathbf{v}'$  is a known and fixed vector in each iteration. Notice that the gradient of the objective

$$\nabla_{\mathbf{b}}\Phi(\mathbf{b}) = \frac{2\sqrt{\beta} \operatorname{Re}(\mathbf{C}^H \mathbf{C} \mathbf{b})}{\|\mathbf{C} \mathbf{b}\|_2} - \mathbf{q} \quad (40)$$

is unbounded when  $\|\mathbf{C} \mathbf{b}\|_2 \rightarrow 0$ , which happens if  $\mathbf{b} \in \operatorname{Null}(\mathbf{C})$ . Therefore, it is nontrivial to apply first-order method to problem (39). To avoid the unbounded gradients, we adopt the smoothing technique [37] to replace  $\Phi(\mathbf{b})$  in (39) with

$$\Xi(\mathbf{b}) = 2\sqrt{\beta} \times \sqrt{\phi^2 + \|\mathbf{C} \mathbf{b}\|_2^2} - \mathbf{q}^T \mathbf{b}, \quad (41)$$

where the tuning parameter  $\phi \geq 0$  such that  $\Xi(\mathbf{b}) = \Phi(\mathbf{b})$  for  $\phi = 0$ . Then problem (39) can be approximated by

$$\mathcal{Q}_2 : \min_{\mathbf{b} \in \Delta} \Xi(\mathbf{b}). \quad (42)$$

In the following, we first elaborate the optimal solution of problem  $\mathcal{Q}_2$ , and then establish the relation between the solutions of problems  $\mathcal{Q}_2$  and (39). First of all, we have the following lemma on the objective of problem  $\mathcal{Q}_2$ .

**Lemma 2.**  $\Xi(\mathbf{b})$  is Lipschitz smooth for  $\mathbf{b} \in \Delta$ , with the Lipschitz constant of gradient

$$L_{\Xi}(\phi) = \frac{2\sqrt{\beta} \lambda_{\max}[\operatorname{Re}(\mathbf{C}^H \mathbf{C})]}{\sqrt{\phi^2 + \lambda_{\min}(\mathbf{C}^H \mathbf{C})/K}}. \quad (43)$$

*Proof.* See Appendix C. ■

Lemma 2 shows that  $\mathcal{Q}_2$  is a Lipschitz smooth problem. As a result, the acceleration method [38], [39] can be adopted to optimally solve  $\mathcal{Q}_2$  iteratively. The algorithm is summarized in Theorem 2.

**Theorem 2.** Let  $\mathbf{b}(0) \in \Delta$  and

$$\mathbf{b}(m+1) = \Pi_{\Delta} \left[ \boldsymbol{\rho}(m) - \frac{1}{L_{\Xi}(\phi)} \nabla_{\mathbf{b}} \Xi(\mathbf{b}) \Big|_{\mathbf{b}=\boldsymbol{\rho}(m)} \right], \quad (44)$$

where  $m$  is the iteration index,  $\Pi_{\Delta}$  is the projection onto set  $\Delta$ ,  $L_{\Xi}(\phi)$  is defined in (43), and

$$\nabla_{\mathbf{b}} \Xi(\mathbf{b}) = \mathbf{q} - 2\sqrt{\beta} \times \frac{\operatorname{Re}(\mathbf{C}^H \mathbf{C} \mathbf{b})}{\sqrt{\phi^2 + \|\mathbf{C} \mathbf{b}\|_2^2}}, \quad (45)$$

$$\boldsymbol{\rho}(m) = \mathbf{b}(m) + \frac{c(m-1)-1}{c(m)} (\mathbf{b}(m) - \mathbf{b}(m-1)), \quad (46)$$

$$c(m) = \frac{1}{2} \left( 1 + \sqrt{1 + 4(c(m-1))^2} \right), \quad c(0) = 1. \quad (47)$$

Then the sequence computed from (44)–(47) converges to the optimal solution of  $\mathcal{Q}_2$  with an iteration complexity  $\mathcal{O}\left(\sqrt{L_{\Xi}(\phi)/\epsilon}\right)$ , where  $\epsilon$  is the target accuracy.

*Proof.* It can be proved by following a similar approach in [39, Theorem 4.4]. ■

Notice that the iteration complexity touches the lower bound derived in [40, Theorem 2.1.6]. The computation of the projection  $\Pi_{\Delta}(\mathbf{u})$  given the input vector  $\mathbf{u}$  is summarized in Lemma 3.

**Lemma 3.** Let  $\mathbf{u}' = \text{sort}(\mathbf{u})$ , where the function *sort* permutes the elements of  $\mathbf{u}$  in a descent order such that  $u'_1 \geq \dots \geq u'_K$  and  $\delta = \max_{x \in \{1, \dots, K\}} \left\{ x : \frac{\sum_{l=1}^x u'_l - 1}{x} < u'_x \right\}$ . Then

$$\Pi_{\Delta}(\mathbf{u}) = \left( \mathbf{u} - \frac{\sum_{l=1}^{\delta} u'_l - 1}{\delta} \right)^+. \quad (48)$$

*Proof.* Please refer to [41, Proposition 2.2] and is omitted for brevity. ■

Finally, we have the following conclusion on the relation between the solutions to problems  $\mathcal{Q}_2$  and (39).

**Theorem 3.** (i) If  $\text{Rank}([\mathbf{g}_1, \dots, \mathbf{g}_K]) = K$  (thus  $L_{\Xi}(0) < +\infty$ ), the optimal solution to problem  $\mathcal{Q}_2$  is optimal to problem (39) by setting  $\phi = 0$ . (ii) If  $\text{Rank}([\mathbf{g}_1, \dots, \mathbf{g}_K]) \neq K$ , then  $L_{\Xi}(0) = +\infty$ , and  $L_{\Xi}(\phi) < +\infty$  if  $\phi > 0$ . (iii) For all  $\mathbf{b}' \in \Delta$  with  $\Xi(\mathbf{b}') - \Xi(\mathbf{b}^{\diamond}) \leq \epsilon$ ,

$$\Phi(\mathbf{b}') - \Phi(\mathbf{b}^*) \leq 2\sqrt{\beta}\phi + \epsilon, \quad (49)$$

where  $\mathbf{b}^{\diamond}$  and  $\mathbf{b}^*$  denote the optimal solutions to  $\mathcal{Q}_2$  and (39), respectively.

*Proof.* See Appendix D. ■

Part (i) of Theorem 3 indicates that we can always set  $\phi = 0$  if the user channels are independent. In this case,  $\Phi(\mathbf{b}) = \Xi(\mathbf{b})$ , which means that the optimal solution to problem  $\mathcal{Q}_2$  is the same as that of (39). On the other hand, part (ii) of Theorem 3 indicates that if the user channels are correlated, we must choose  $\phi > 0$ , and the conversion from (39) to  $\mathcal{Q}_2$  would lead to approximation error. However, this error is controllable by choosing a small  $2\sqrt{\beta}\phi$  according to part (iii) of Theorem 3 (e.g., with  $\phi = 0.1/(2\sqrt{\beta})$ , the approximation error is  $2\sqrt{\beta}\phi = 0.1$ ).

### C. Summary and Complexity Analysis of AGP

For the proposed AGP algorithm, the accelerated random coordinate descent is first used to compute  $\mathbf{w}^\diamond$  for problem on the right hand side of the constraint in (32), which requires a complexity of  $\mathcal{O}(KN)$ . To optimize  $\mathbf{v}^\diamond$ , in each fixed-point iteration, the terms  $\mathbf{C}$  in (37) and  $\mathbf{q}$  in (38) are computed with a complexity of  $\mathcal{O}(KN)$ , followed by the iterative calculation of variable  $\mathbf{b}$  in (39) with equations (44)–(47), which involves a complexity of  $\mathcal{O}(KN)$  for gradient computation. Therefore, the overall complexity of AGP for solving  $\mathcal{Q}$  is  $\mathcal{O}(KN)$ . Notice that with the obtained  $\mathbf{w}^\diamond$  and  $\mathbf{v}^\diamond$ , we need to recover  $\{\mathbf{F}^*, r_k^*, t_k^*\}$ . To satisfy the unit-modulus constraints,  $\mathbf{w}^\diamond$  and  $\mathbf{v}^\diamond$  are refined into  $\mathbf{w}^* = \exp(j\angle \mathbf{w}^\diamond)$  and  $\mathbf{v}^* = \exp(j\angle \mathbf{v}^\diamond)$ . The final solution is given by  $t_k^* = 1/(K(\mathbf{w}^*)^H \mathbf{h}_k)$  and  $\mathbf{F}^* = (\mathbf{w}^*)^H \mathbf{v}^*$ . With  $t_k^*$  and  $\mathbf{F}^*$ ,  $r_k^*$  is computed using (26).

*Remark 3 (Number of Phase Shifters):* For the UM-AirComp scheme with AGP, the analog beamforming matrix  $\mathbf{F}^* = (\mathbf{w}^*)^H \mathbf{v}^*$  is rank-one. Therefore, it only costs  $2N$  phase shifters at the edge server, which is significantly smaller than  $N^2$  phase shifters used in PAM-based UM-AirComp scheme. Hence, it is particularly suitable for FL systems with massive antenna arrays at the edge. In practice, the number of phase shifters can also take the values of  $(4N, 6N \dots)$  by varying the number of RF chains.

## VI. SIMULATION RESULTS AND DISCUSSIONS

This section presents simulation results to verify the performance of the proposed scheme. The pathloss of the user  $k$  is set to  $\varrho_k = -60$  dB, and  $\mathbf{h}_k$  and  $\mathbf{g}_k$  are generated according to  $\mathcal{CN}(\mathbf{0}, \varrho_k \mathbf{I}_N)$ . The power scaling factor  $\gamma = 1$  and the maximum transmit powers at users are  $P_0 = 10$  mW (i.e., 10 dBm). The number of local updates  $E = 1$ . The noise powers at the server and users are set as  $-90$  dBm, which capture the effects of thermal noise, receiver noise, and interference. Each point of MSE is obtained by averaging over 100 runs, with independent channel and noise realization in each run. All problems are solved by Matlab R2019a on a desktop with an Intel Core i7-7700 CPU at 3.6 GHz and 16 GB RAM. The Interior point method is implemented using CVX Mosek [32], a Matlab software package for convex optimization.

### A. Performance Evaluation of PAM-based and AGP-based UM-AirComp

First, the convergence behavior of the proposed PAM is demonstrated. According to Section IV, PAM consists of two iteration layers. To verify the convergence of the inner layer (i.e., equations

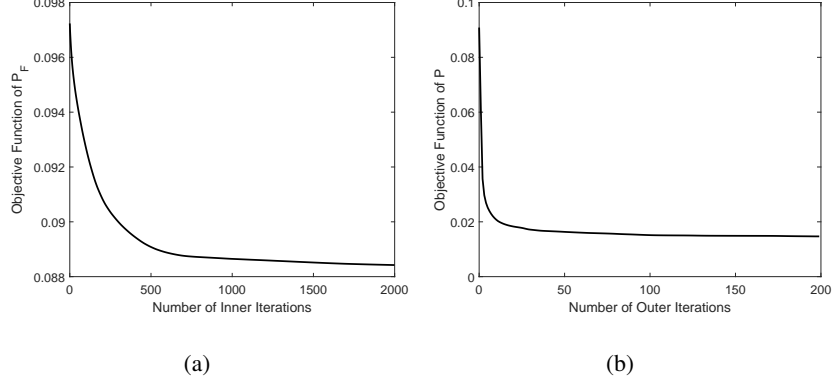


Fig. 3: a) the objective function of  $\mathcal{P}_F$  versus the number of inner iterations  $m$  at  $n = 0$  when  $N = 8$ ; b) the objective function of  $\mathcal{P}$  versus the number of outer iterations  $n$  when  $N = 8$ .

(22)–(24)) of the proposed PAM, Fig. 3a shows the objective function of  $\mathcal{P}_F$  (i.e. (19)) versus the number of inner iterations  $m = (1, \dots, 2000)$  at  $n = 0$  when  $N = 8$  and  $K = 10$ . It can be seen that the inner layer for updating  $\mathbf{F}$  converges after 1500 iterations with  $\rho = 0.1$ . Besides, since the convergence behaviors for equations (28)–(29) are similar, they are not repeated here. On the other hand, to verify the convergence of the outer layer (i.e., equations (16a)–(16c)) of the proposed PAM, Fig. 3b shows the objective function of  $\mathcal{P}$  (i.e. (15a)) versus the number of outer iterations  $n = (1, \dots, 200)$ . As observed from the figure, the proposed algorithm converges and the MSE stabilizes after 50 iterations, which indicates that the number of outer iterations  $N_{\max}$  for PAM to converge is small. To reduce the runtime in practice, the inner and outer problems can both be solved approximately, and we set  $M_{\max} = 200$  and  $N_{\max} = 20$  in the subsequent simulations.

Next, to verify the learning performance of PAM-based UM-AirComp, we consider three benchmark schemes:

- 1) Baseline scheme, which sets  $\mathbf{F} = \mathbf{I}_N$  and  $\{t_k = \sqrt{P_0}|\forall k\}$ . The receiver coefficients  $\{r_k\}$  are computed using (26).
- 2) The fixed beamforming scheme, which sets  $\mathbf{F} = \mathbf{I}_N$ . The transmitter coefficients  $\{t_k\}$  and receiver coefficients  $\{r_k\}$  are optimized iteratively by solving (16c) using CVX and (16b) using (26), respectively.
- 3) The UM-AirComp scheme with SDR and CVX. The analog beamformer  $\mathbf{F}$ , the transmitter coefficients  $\{t_k\}$ , and the receiver coefficients  $\{r_k\}$  are optimized iteratively by solving

(16a) using SDR, (16c) using CVX, and (16b) using (26), respectively.<sup>4</sup>

We simulate the deep learning task of Example 2 mentioned in Section II. It is assumed that the channel coherence time lasts for 10 FL iterations and the total number of FL iterations is set to 1000. The result is shown in Fig. 4. Specifically, the axis limits of the radar map in Fig. 4a are (0.0972, 1.8996, 0.9540, 49.6140) for normalized MSE (i.e., the objective function of  $\mathcal{P}$ ), training loss in (1), testing error, and computation time, respectively. Since our goal is to minimize all these metrics concurrently, a smaller area indicates better performance. It can be seen from Fig. 4a that the proposed PAM-based UM-AirComp scheme achieves the smallest area among all the simulated schemes. In particular, the area of the proposed scheme is completely covered by that of the fixed beamforming scheme, and the area reduction comes from the analog beamforming design and the low complexity nature of PAM. The scheme with SDR and CVX is the most time consuming, making it not applicable in practice. On the other hand, although the baseline scheme is the fastest, it has the highest MSE, training loss, and test error.

Fig. 4b and Fig. 4c show the training loss and the testing error versus the number of FL iterations, respectively. Due to the high MSE (close to 0.1), FL with the baseline scheme diverges. The FL with fixed beamforming is competitive compared with the proposed scheme at the beginning, but the training loss does not further reduce with the increasing number of FL iterations. Besides, the test error increases after 600 iterations. This means that model parameter errors have a stronger impact as the number of FL iterations increases. This is because deep learning models are usually over parameterized. Thus, as the training procedure gets closer to convergence, the model parameters would get sparser, which are more sensitive to model parameter errors. Based on the above observations, we can adopt an approximate solution (e.g., executing few iterations of the PAM algorithm) for edge FL designs at the early stage and switch to high-performance solution (e.g., executing PAM algorithm until convergence) at the latter stage. On the other hand, the scheme with SDR and CVX has the same performance as the proposed scheme. However, as indicated in Fig. 4a, it requires a much higher runtime.

To evaluate the solution quality and runtime of the proposed AGP-based UM-AirComp, we simulate the case of  $N = \{8, 16, 64, 256\}$  with  $K = 4$ . It can be seen from Fig. 5a that the scheme with SDR and CVX is the most time consuming, and it fails in providing a solution

<sup>4</sup>If the matrix solution to the SDR problem of (16a) is not rank-one, we use the principal component of the obtained matrix as the phase shift design.

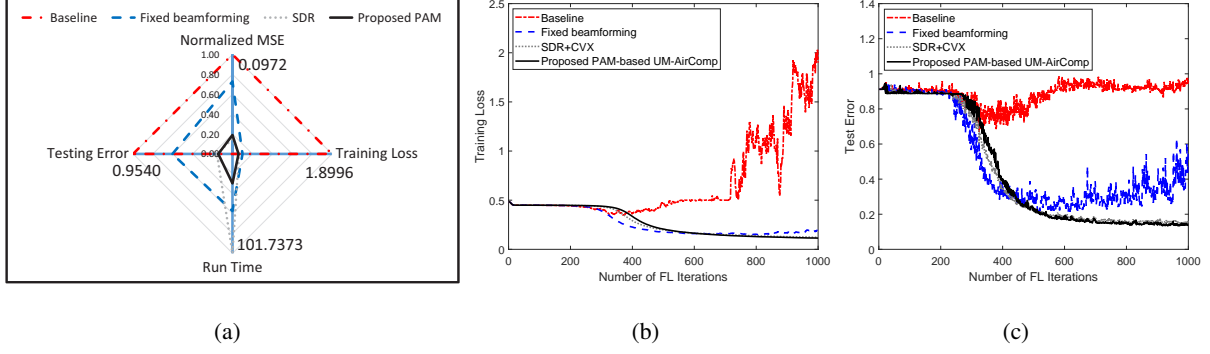


Fig. 4: Comparison between the proposed and benchmark schemes when  $N = 8$  with  $K = 10$ : a) comparison of normalized MSE, training loss, test error, and runtime; b) training loss versus the number of FL iterations; c) worst test error among all users versus the number of FL iterations.

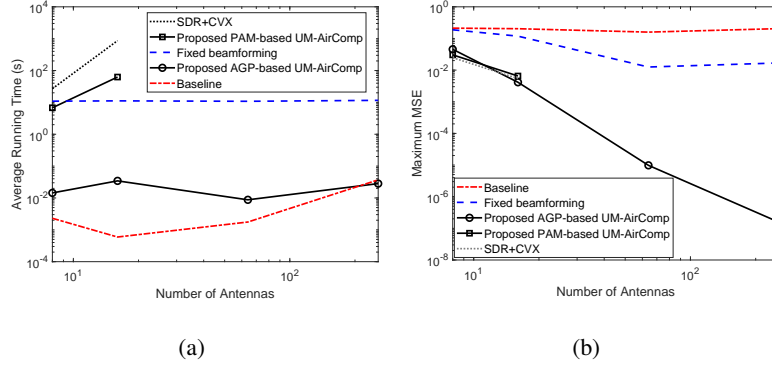


Fig. 5: Run time and normalized MSE versus the number of antennas when  $K = 4$ .

within a reasonable amount of time for the case of  $N = \{64, 256\}$ . Note that the proposed PAM-based UM-AirComp, although faster than SDR method, still requires a high runtime at  $N = \{64, 256\}$ . On the other hand, the proposed AGP-based UM-AirComp and the baseline scheme require runtimes two orders of magnitude smaller than that of other schemes. However, as shown in Fig. 5b, the proposed AGP-based UM-AirComp significantly outperforms that of the baseline.

### B. UM-AirComp for V2X Autonomous Driving

Finally, to verify the robustness of the proposed UM-AirComp framework in complex learning tasks, we consider the V2X-aided FL for 3D object detection. We employ the CARLA simulation platform [24] to generate training/testing scenarios and multi-agent point cloud datasets. Each



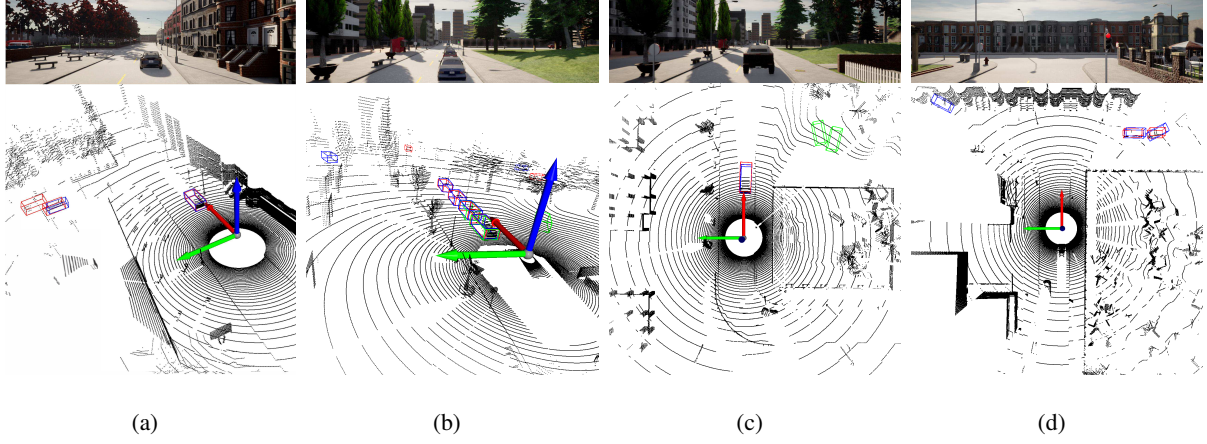


Fig. 6: Detection results when  $N = 500$  with  $K = 4$ . The red box is the ground truth; the blue box is from the proposed AGP-based UM-AirComp scheme; the green box is from the fixed beamforming (benchmark) scheme. a) the benchmark scheme detects nothing while the proposed scheme detects two objects; b) the benchmark scheme only detects two nearby objects while the proposed scheme can detect far-away objects; c) the benchmark scheme generates false positive results while the proposed scheme generates accurate prediction; d) the benchmark scheme cannot detect occlusion objects while the proposed scheme detects all of them.

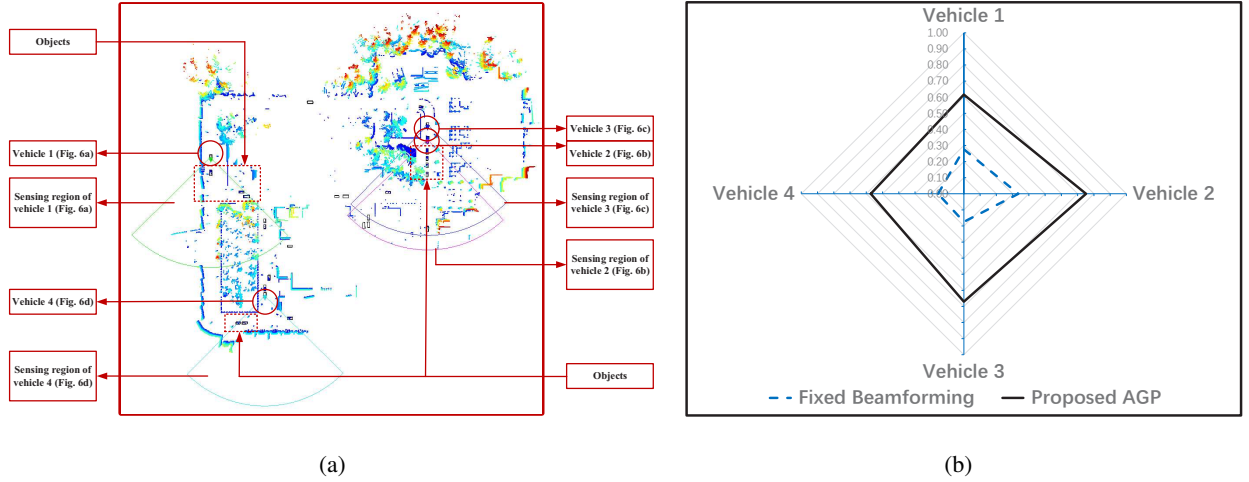


Fig. 7: a) The global bird eye view of the frame in Fig. 6. The green vehicle is in Fig. 6a. The pink vehicle is in Fig. 6b. The blue vehicle is in Fig. 6c. The cyan vehicle is in Fig. 6d. b) Comparison between the proposed AGP-based UM-AirComp and the fixed beamforming schemes when  $N = 500$  with  $K = 4$ .

intelligent vehicle (Tesla Model 3) is equipped with a 64-line LiDAR at 10 Hz. The default LiDAR range is set to 100 m, and its FoV is  $90^\circ$  in the front. We use the “Town02” map [24] with 28 objects and 4 autonomous vehicles. The entire scenario lasts for 90 seconds and contains 900 frames at each autonomous vehicle. The first 400 frames are used for FL training. The sampling rate is 1/2 and hence 200 frames are used for training at each vehicle. The latter 500 frames are used for inference and testing. Each frame is considered as a input data  $\mathbf{d}_l^{\text{in}}$ , which consists of around 100,000 points and each point has 3 coordinates. The corresponding object labels  $\mathbf{d}_l^{\text{out}} = \{[c_m, x_m, y_m, z_m, l_m, w_m, h_m, \vartheta_m]^T\}_{m=1}^M$ , where  $M$  is the number of objects,  $c_m$  is the category,  $(x_m, y_m, z_m)$  are the center coordinates,  $(l_m, w_m, h_m)$  stand for the length, width, and height, and  $\vartheta_m$  denotes the yaw rotation around the z-axis of the  $m$ -th object, respectively. Thus each sample is  $\mathbf{d}_l = (\mathbf{d}_l^{\text{in}}, \mathbf{d}_l^{\text{out}}) \in \{\mathcal{D}_1, \dots, \mathcal{D}_K\}$ . The average precision at IoU= 0.5 is used for performance evaluation.

The sparsely embedded convolutional detection (SECOND) neural network [21] is used for object detection on the CARLA dataset. The local model structure can be found in [21]. The loss function  $\Theta(\mathbf{d}_l, \mathbf{x}_k) = f_{\text{class}}(\mathbf{x}_k, \mathbf{d}_l^{\text{in}}, \{c_m\}) + f_{\text{box}}(\mathbf{x}_k, \mathbf{d}_l^{\text{in}}, \{x_m, y_m, z_m, l_m, w_m, h_m\}) + f_{\text{soft}}(\mathbf{x}_k, \mathbf{d}_l^{\text{in}}, \{\vartheta_m\})$ , where  $f_{\text{class}}$  is the classification loss,  $f_{\text{box}}$  is the box regression loss, and  $f_{\text{soft}}$  is the softmax orientation estimation loss. Since the multi-agent data generated by CARLA is not compatible to the SECOND network, we develop a data transformation module such that the generated dataset satisfies the KITTI standard [25]. The SECOND network is trained with a diminishing learning rate, where the initial learning rate is set to  $10^{-4}$  and the number of local updates is  $E = 1$ . The experiment is done using Python 3.6 in Ubuntu 18.04 with a GeForce GTX 3090 GPU.

In our experiment, the case of  $N = 500$  and  $K = 4$  is simulated. It is assumed that the sensing datasets are generated and pre-stored at the vehicles before transmission. The channels  $\{\mathbf{h}_k, \mathbf{g}_k\}$  are randomly generated according to  $\mathcal{CN}(\mathbf{0}, \varrho_k \mathbf{I}_N)$  with a pathloss of  $\varrho_k = -60$  dB. The total number of FL iterations is 8, with independently generated channel in each FL iteration. For autonomous vehicles, its transmit power is larger than IoT devices. Thus we set  $P_0 = 30$  mW (i.e., 1 W), and the noise powers remain the same as above subsections. The normalized MSEs of the proposed AGP-based UM-AirComp and the fixed beamforming (benchmark) schemes are  $6 \times 10^{-11}$  and 0.0013, respectively. The detection results are shown in Fig. 6 and the global bird eye view of this frame is shown in Fig. 7a. The comparison between the proposed and benchmark schemes is provided in Fig. 7b.

From the above results, it can be seen that the MSEs of both schemes are remarkably smaller than their counterparts in Fig. 4a. However, the learning performance of Fig. 6 and Fig. 7b is worse than that in Fig. 4b and Fig. 4c, which implies that object detection tasks in autonomous driving are more sensitive to model parameter errors. This is because the trained model parameters for the SECOND network are generally sparser and a slight model error would lead to completely different predictions. Furthermore, as seen from the objective of  $\mathcal{P}$ , the model error of user  $k$  with the UM-AirComp framework is dominated by  $\gamma \sum_{j=1}^K \left| r_k \mathbf{g}_k^H \mathbf{F} \mathbf{h}_j t_j - \alpha_j \right|^2$ . Therefore, the methods to minimize the model errors can be categorized into 1) configuration of wireless channels  $\{\mathbf{h}_k, \mathbf{g}_k\}$  and 2) design of analog beamformer  $\mathbf{F}$ . For the configuration of wireless channels, due to  $\alpha_1 = \dots = \alpha_K$ , the ideal wireless channels for the proposed UM-AirComp satisfy  $\mathbf{g}_1 = \dots = \mathbf{g}_K$  and  $\mathbf{h}_1 = \dots = \mathbf{h}_K$ . This implies that the UM-AirComp should be executed when vehicles are geographically close to each other such that the magnitudes of  $\{\mathbf{h}_k, \mathbf{g}_k\}$  are close. This is the case in vehicle platooning and vehicle parking scenarios [45]; otherwise, some emerging techniques (e.g., reconfigurable intelligence surfaces (RIS) [5]) should be adopted to smartly alter the wireless environment. On the other hand, for the design of beamformers, the key is to align the various channels  $\{\mathbf{h}_k, \mathbf{g}_k\}$  to a same direction and power for decoding superposed signals. This is the case of Fig. 7b, where the proposed method achieves much larger average precisions than the fixed beamforming scheme for all vehicles. Note that the runtime of AGP-based UM-AirComp is only 0.06 s, which can be further accelerated via dedicated GPU.

## VII. CONCLUSION

This paper proposed the UM-AirComp scheme to support simultaneous transmission of local model parameters in edge federated learning systems. The training loss upper bound of UM-AirComp was derived, which reveals that the key to minimize FL training loss is to minimize the maximum MSE among all users. Two low-complexity large-scale optimization algorithms were proposed to tackle the nonconvex nonsmooth loss bound minimization problem. The performance and runtime of the UM-AirComp framework with the proposed optimization algorithms were verified using regression and classification tasks. The performance of the proposed framework and algorithms were also verified in a V2X autonomous driving simulation platform and experimental results have shown that the object detection precision with the proposed algorithm is significantly higher than that achieved by benchmark schemes.

APPENDIX A  
PROOF OF THEOREM 1

To prove the theorem, we will first show that  $\mathbb{E} [\|\Delta \mathbf{x}^{[i]}\|_2^2] \leq (3 + 2K^{-1}) \max_k \text{MSE}_k^{[i]}$ , where  $\Delta \mathbf{x}^{[i]} = \mathbf{x}_k^{[i+1]}(0) - [\mathbf{x}_k^{[i]}(0) - \varepsilon \nabla_{\mathbf{x}} \Lambda(\mathbf{x}_k^{[i]}(0))]$ . Then, using Assumption 1 and Lipschitz conditions, the relationship between  $\Lambda(\mathbf{x}_k^{[i+1]}(0)) - \Lambda(\mathbf{x}_k^{[i]}(0))$  and  $\mathbb{E} [\|\Delta \mathbf{x}^{[i]}\|_2^2]$  is obtained. Lastly, applying the former relationship recursively, the relationship between  $\mathbb{E} [\Lambda(\mathbf{x}_k^{[i+1]}(0)) - \Lambda(\boldsymbol{\theta}^*)]$  and  $\mathbb{E} [\|\Delta \mathbf{x}^{[i]}\|_2^2]$  is obtained. The details are given below.

**1) Bounding  $\|\Delta \mathbf{x}^{[i]}\|_2^2$ .** We first derive the following upper bound

$$\begin{aligned} \|\Delta \mathbf{x}^{[i]}\|_2^2 &= \left\| \mathbf{x}_k^{[i+1]}(0) - \mathbf{x}_k^{[i]}(0) + \varepsilon \nabla_{\mathbf{x}} \Lambda(\mathbf{x}_k^{[i]}(0)) \right\|_2^2 \\ &= \left\| \mathbf{x}_k^{[i+1]}(0) - \boldsymbol{\theta}^{[i]} + \sum_{j=1}^K \alpha_j \mathbf{x}_j^{[i]}(0) - \frac{\varepsilon}{\sum_{j=1}^K |\mathcal{D}_j|} \sum_{j=1}^K \sum_{\mathbf{d}_l \in \mathcal{D}_j} \nabla_{\mathbf{x}} \Theta(\mathbf{d}_l, \mathbf{x}_j^{[i]}(0)) \right. \\ &\quad \left. - \mathbf{x}_k^{[i]}(0) + \varepsilon \nabla_{\mathbf{x}} \Lambda(\mathbf{x}_k^{[i]}(0)) \right\|_2^2 \\ &\leq \left\| \mathbf{x}_k^{[i+1]}(0) - \boldsymbol{\theta}^{[i]} \right\|_2^2 + \sum_{j=1}^K \alpha_j \left\| \mathbf{x}_j^{[i]}(0) - \mathbf{x}_k^{[i]}(0) \right\|_2^2 \\ &\quad + \frac{\varepsilon^2}{(\sum_{j=1}^K |\mathcal{D}_j|)^2} \sum_{j=1}^K \left\| \sum_{\mathbf{d}_l \in \mathcal{D}_j} \nabla_{\mathbf{x}} \Theta(\mathbf{d}_l, \mathbf{x}_j^{[i]}(0)) - \sum_{\mathbf{d}_l \in \mathcal{D}_j} \nabla_{\mathbf{x}} \Theta(\mathbf{d}_l, \mathbf{x}_k^{[i]}(0)) \right\|_2^2, \quad (50) \end{aligned}$$

where the second equality is obtained from (2) with  $E = 1$  and (6), and the inequality is obtained due to  $\|\mathbf{a}_1 + \mathbf{a}_2\|_2^2 \leq \|\mathbf{a}_1\|_2^2 + \|\mathbf{a}_2\|_2^2$ . On the other hand, according to (11), we have

$$\begin{aligned} \mathbb{E} \left[ \left\| \mathbf{x}_k^{[i+1]}(0) - \boldsymbol{\theta}^{[i]} \right\|_2^2 \right] &= \text{MSE}_k^{[i]}, \\ \mathbb{E} \left[ \left\| \mathbf{x}_k^{[i]}(0) - \mathbf{x}_j^{[i]}(0) \right\|_2^2 \right] &= \mathbb{E} \left[ \left\| \mathbf{x}_k^{[i]}(0) - \boldsymbol{\theta}^{[i-1]} + \boldsymbol{\theta}^{[i-1]} - \mathbf{x}_j^{[i]}(0) \right\|_2^2 \right] \leq 2\text{MSE}_k^{[i]}. \quad (51) \end{aligned}$$

Moreover, according to Assumption 1, we have

$$\begin{aligned} &\mathbb{E} \left[ \left\| \sum_{\mathbf{d}_l \in \mathcal{D}_j} \nabla_{\mathbf{x}} \Theta(\mathbf{d}_l, \mathbf{x}_j^{[i]}(0)) - \sum_{\mathbf{d}_l \in \mathcal{D}_j} \nabla_{\mathbf{x}} \Theta(\mathbf{d}_l, \mathbf{x}_k^{[i]}(0)) \right\|_2^2 \right] \\ &\leq \mathbb{E} \left[ L^2 \|\mathbf{x}_k^{[i]}(0) - \mathbf{x}_j^{[i]}(0)\|_2^2 \right] \\ &\leq 2L^2 \text{MSE}_k^{[i]}. \quad (52) \end{aligned}$$

Putting (51) and (52) into (50), and according to the expression of  $\varepsilon$  yields

$$\mathbb{E} [\|\Delta \mathbf{x}^{[i]}\|_2^2] \leq (3 + 2K^{-1}) \max_{k=1, \dots, K} \text{MSE}_k^{[i]}. \quad (53)$$

**2) Bounding**  $\Lambda(\mathbf{x}_k^{[i+1]}(0)) - \Lambda(\mathbf{x}_k^{[i]}(0))$ . Due to  $\sum_{\mathbf{d}_l \in \mathcal{D}_k} \nabla_{\mathbf{x}}^2 \Theta(\mathbf{d}_l, \mathbf{x}) \preceq L\mathbf{I}$ , we have  $\nabla_{\mathbf{x}}^2 \Lambda(\mathbf{x}) \preceq KL/(\sum_k |\mathcal{D}_k|)\mathbf{I}$ . Based on  $\mu\mathbf{I} \preceq \nabla_{\mathbf{x}}^2 \Lambda(\mathbf{x}) \preceq KL/(\sum_k |\mathcal{D}_k|)\mathbf{I}$ , the following equations hold [40]:

$$\Lambda(\mathbf{x}') \leq \Lambda(\mathbf{x}) + (\mathbf{x}' - \mathbf{x})^T \nabla \Lambda(\mathbf{x}) + \frac{KL}{2 \sum_{k=1}^K |\mathcal{D}_k|} \|\mathbf{x}' - \mathbf{x}\|_2^2, \quad (54a)$$

$$\Lambda(\mathbf{x}') \geq \Lambda(\mathbf{x}) + (\mathbf{x}' - \mathbf{x})^T \nabla \Lambda(\mathbf{x}) + \frac{\mu}{2} \|\mathbf{x}' - \mathbf{x}\|_2^2. \quad (54b)$$

Putting  $\mathbf{x}' = \mathbf{x}_k^{[i+1]}(0) = \mathbf{x}_k^{[i]}(0) - \varepsilon \nabla_{\mathbf{x}} \Lambda(\mathbf{x}_k^{[i]}(0)) + \Delta \mathbf{x}^{[i]}$  and  $\mathbf{x} = \mathbf{x}_k^{[i]}(0)$  into (54a), we have

$$\Lambda(\mathbf{x}_k^{[i+1]}(0)) \leq \Lambda(\mathbf{x}_k^{[i]}(0)) - \frac{\sum_{j=1}^K |\mathcal{D}_j|}{2KL} \left\| \nabla_{\mathbf{x}} \Lambda(\mathbf{x}_k^{[i]}(0)) \right\|_2^2 + \frac{KL}{2 \sum_{j=1}^K |\mathcal{D}_j|} \|\Delta \mathbf{x}^{[i]}\|_2^2. \quad (55)$$

On the other hand, the right hand side of (54b) is minimized at  $\mathbf{x}' = \mathbf{x} - \mu^{-1} \nabla_{\mathbf{x}} \Lambda(\mathbf{x})$ . Putting this expression and  $\mathbf{x} = \mathbf{x}_k^{[i]}(0)$  into (54b) gives

$$\left\| \nabla_{\mathbf{x}} \Lambda(\mathbf{x}_k^{[i]}(0)) \right\|_2^2 \geq 2\mu \left[ \Lambda(\mathbf{x}_k^{[i]}(0)) - \Lambda(\boldsymbol{\theta}^*) \right]. \quad (56)$$

Combining (55) and (56) gives

$$\Lambda(\mathbf{x}_k^{[i+1]}(0)) - \Lambda(\mathbf{x}_k^{[i]}(0)) \leq \left( 1 - \frac{\mu \sum_{j=1}^K |\mathcal{D}_j|}{KL} \right) \left[ \Lambda(\mathbf{x}_k^{[i]}(0)) - \Lambda(\boldsymbol{\theta}^*) \right] + \frac{KL}{2 \sum_{j=1}^K |\mathcal{D}_j|} \|\Delta \mathbf{x}^{[i]}\|_2^2. \quad (57)$$

**3) Bounding**  $\mathbb{E} \left[ \Lambda(\mathbf{x}_k^{[i+1]}(0)) - \Lambda(\boldsymbol{\theta}^*) \right]$ . Applying (57) recursively leads to

$$\begin{aligned} \Lambda(\mathbf{x}_k^{[i+1]}(0)) - \Lambda(\boldsymbol{\theta}^*) &\leq \left( 1 - \frac{\mu \sum_{j=1}^K |\mathcal{D}_j|}{KL} \right)^{i+1} \left[ \Lambda(\mathbf{x}_k^{[0]}(0)) - \Lambda(\boldsymbol{\theta}^*) \right] \\ &\quad + \sum_{i'=0}^i \frac{KL}{2 \sum_{j=1}^K |\mathcal{D}_j|} \left( 1 - \frac{\mu \sum_{j=1}^K |\mathcal{D}_j|}{KL} \right)^{i-i'} \|\Delta \mathbf{x}^{[i']}\|_2^2. \end{aligned} \quad (58)$$

Taking expectation on both sides and applying (53), (58) becomes

$$\begin{aligned} \mathbb{E} \left[ \Lambda(\mathbf{x}_k^{[i+1]}(0)) - \Lambda(\boldsymbol{\theta}^*) \right] &\leq \left( 1 - \frac{\mu \sum_{j=1}^K |\mathcal{D}_j|}{KL} \right)^{i+1} \left[ \Lambda(\mathbf{x}_k^{[0]}(0)) - \Lambda(\boldsymbol{\theta}^*) \right] \\ &\quad + \sum_{i'=0}^i A^{[i']} \max_k \text{MSE}_k^{[i']}. \end{aligned} \quad (59)$$

Finally, taking the limit  $i \rightarrow +\infty$  and using  $\left( 1 - \mu \sum_{j=1}^K |\mathcal{D}_j| / (KL) \right)^{i+1} \rightarrow 0$ , the proof is completed.

## APPENDIX B

### PROOF OF LEMMA 1

The lemma is proved by showing that  $U(\mathbf{v}')$  is the optimal solution to

$$\min_{\|\mathbf{v}\|_2^2 \leq \beta} \max_{\mathbf{b} \in \Delta} g(\mathbf{v}, \mathbf{v}', \mathbf{b}), \quad (60)$$

where  $g(\mathbf{v}, \mathbf{v}', \mathbf{b})$  is a function satisfying  $g(\mathbf{v}, \mathbf{v}', \mathbf{b}) \geq h(\mathbf{v}, \mathbf{b})$ ,  $g(\mathbf{v}', \mathbf{v}', \mathbf{b}) = h(\mathbf{v}', \mathbf{b})$ , and  $\nabla g(\mathbf{v}', \mathbf{v}', \mathbf{b}) = \nabla h(\mathbf{v}', \mathbf{b})$ . Then according to [35] and the properties of  $g(\mathbf{v}, \mathbf{v}', \mathbf{b})$ , every limit point of the sequence  $(\mathbf{v}^{(0)}, \mathbf{v}^{(1)}, \dots)$  generated by  $\mathbf{v}^{(n+1)} \leftarrow U(\mathbf{v}^{(n)})$  and a feasible  $\mathbf{v}^{(0)}$  is the KKT solution to (34).

Specifically, define a surrogate function of  $h(\mathbf{v}, \mathbf{b})$  as

$$g(\mathbf{v}, \mathbf{v}', \mathbf{b}) = - \sum_{k=1}^K \frac{b_k |\mathbf{g}_k^H \mathbf{v}|^2}{\sigma_k^2} + \sum_{k=1}^K \frac{b_k (\mathbf{v} - \mathbf{v}')^H \mathbf{g}_k \mathbf{g}_k^H (\mathbf{v} - \mathbf{v}')}{\sigma_k^2}. \quad (61)$$

It can be verified that  $g(\mathbf{v}, \mathbf{v}', \mathbf{b}) \geq h(\mathbf{v}, \mathbf{b})$ ,  $g(\mathbf{v}', \mathbf{v}', \mathbf{b}) = h(\mathbf{v}', \mathbf{b})$ , and  $\nabla g(\mathbf{v}', \mathbf{v}', \mathbf{b}) = \nabla h(\mathbf{v}', \mathbf{b})$ . Therefore, to prove the lemma, it remains to show that  $U(\mathbf{v}')$  is the optimal solution to (60) with  $g(\mathbf{v}, \mathbf{v}', \mathbf{b})$  given by (61). Applying the quasi-concave-convex property of (60) and the general minimax theorem [36], we have

$$\min_{\|\mathbf{v}\|_2^2 \leq \beta} \max_{\mathbf{b} \in \Delta} g(\mathbf{v}, \mathbf{v}', \mathbf{b}) = \max_{\mathbf{b} \in \Delta} \min_{\|\mathbf{v}\|_2^2 \leq \beta} g(\mathbf{v}, \mathbf{v}', \mathbf{b}). \quad (62)$$

Via the Lagrange multiplier method, it can be derived that

$$\arg \min_{\|\mathbf{v}\|_2^2 \leq \beta} g(\mathbf{v}, \mathbf{v}', \mathbf{b}) = \frac{\sqrt{\beta} \mathbf{C}(\mathbf{v}') \mathbf{b}}{\|\mathbf{C}(\mathbf{v}') \mathbf{b}\|_2}. \quad (63)$$

Putting the above result into  $g(\mathbf{v}, \mathbf{v}', \mathbf{b})$ , we have

$$g\left(\frac{\sqrt{\beta} \mathbf{C}(\mathbf{v}') \mathbf{b}}{\|\mathbf{C}(\mathbf{v}') \mathbf{b}\|_2}, \mathbf{v}', \mathbf{b}\right) = -\Phi(\mathbf{v}', \mathbf{b}). \quad (64)$$

Therefore, the optimal solution of  $\mathbf{b}$  to (62) is  $\arg \min_{\mathbf{b} \in \Delta} \Phi(\mathbf{v}', \mathbf{b})$ . Putting  $\arg \min_{\mathbf{b} \in \Delta} \Phi(\mathbf{v}', \mathbf{b})$  into (63), the optimal solution of  $\mathbf{v}$  to (62) (thus (60)) is  $U(\mathbf{v}')$  and the proof is completed.

## APPENDIX C

### PROOF OF LEMMA 2

To begin with, we first introduce the following lemma.

**Lemma 4.** ([40, Lemma 1.2.2]) *If  $h(\mathbf{x})$  is convex and twice differentiable, then  $h(\mathbf{x})$  is Lipschitz smooth with constant  $L$  if and only if  $\nabla^2 h(\mathbf{x}) \preceq L \mathbf{I}$ .*

Based on Lemma 4 and since  $\Xi(\mathbf{b})$  is convex and twice differentiable, it suffices to show  $\nabla^2 \Xi(\mathbf{b}) \preceq L_{\Xi}(\phi) \mathbf{I}_K$ . In particular, according to (41), the Hessian matrix of  $\Xi(\mathbf{b})$  is

$$\nabla^2 \Xi(\mathbf{b}) = \frac{2\sqrt{\beta} \operatorname{Re}(\mathbf{C}^H \mathbf{C})}{\sqrt{\phi^2 + \|\mathbf{Cb}\|_2^2}} - \frac{2\sqrt{\beta}}{(\sqrt{\phi^2 + \|\mathbf{Cb}\|_2^2})^3} \times \operatorname{Re}(\mathbf{C}^H \mathbf{Cb}) [\operatorname{Re}(\mathbf{C}^H \mathbf{Cb})]^H.$$

Due to  $\operatorname{Re}(\mathbf{C}^H \mathbf{Cb}) [\operatorname{Re}(\mathbf{C}^H \mathbf{Cb})]^H \succeq \mathbf{0}$ , we can drop the last term to bound  $\nabla^2 \Xi(\mathbf{b})$  from above, which leads to

$$\nabla^2 \Xi(\mathbf{b}) \preceq \frac{2\sqrt{\beta}}{\sqrt{\phi^2 + \|\mathbf{Cb}\|_2^2}} \times \operatorname{Re}(\mathbf{C}^H \mathbf{Cb}) \preceq \frac{2\sqrt{\beta} \cdot \lambda_{\max}[\operatorname{Re}(\mathbf{C}^H \mathbf{C})]}{\sqrt{\phi^2 + \|\mathbf{Cb}\|_2^2}} \mathbf{I}_K, \quad (65)$$

where the second inequality follows from  $\operatorname{Re}(\mathbf{C}^H \mathbf{C}) \preceq \lambda_{\max}[\operatorname{Re}(\mathbf{C}^H \mathbf{C})] \mathbf{I}_K$ .

Now, the only quantity in (65) that is dependent on  $\mathbf{b}$  is  $\|\mathbf{Cb}\|_2^2$ . To get rid of such dependence,  $\|\mathbf{Cb}\|_2^2$  is lower bounded by

$$\|\mathbf{Cb}\|_2^2 = \mathbf{b}^T \mathbf{C}^H \mathbf{Cb} \geq \lambda_{\min}(\mathbf{C}^H \mathbf{C}) \times \|\mathbf{b}\|_2^2. \quad (66)$$

Finally, using  $\|\mathbf{b}\|_2^2 \geq 1/K$  due to  $\mathbf{b} \in \Delta$  and Cauchy-Schwarz inequality further leads to

$$\|\mathbf{Cb}\|_2^2 \geq \lambda_{\min}(\mathbf{C}^H \mathbf{C}) / K. \quad (67)$$

Replacing  $\|\mathbf{Cb}\|_2^2$  in (65) with the right hand side of (67), we immediately obtain  $\nabla^2 \Xi(\mathbf{b}) \preceq L_{\Xi}(\phi) \mathbf{I}_K$ .

## APPENDIX D

### PROOF OF THEOREM 3

To prove part (i) of this theorem, notice that  $\operatorname{Rank}(\mathbf{C}) = \operatorname{Rank}([\mathbf{g}_1, \dots, \mathbf{g}_K])$  due to the definition of  $\mathbf{C}$  in (37). As  $\operatorname{Rank}(\mathbf{C}^H \mathbf{C}) = \operatorname{Rank}(\mathbf{C})$ ,  $\operatorname{Rank}(\mathbf{C}^H \mathbf{C}) = K$  and  $\lambda_{\min}(\mathbf{C}^H \mathbf{C}) > 0$ . Putting  $\lambda_{\min}(\mathbf{C}^H \mathbf{C}) > 0$  and  $\phi = 0$  into (43), we obtain

$$L_{\Xi}(0) = \frac{2\sqrt{\beta} \|\operatorname{Re}(\mathbf{C}^H \mathbf{C})\|_2}{\sqrt{\lambda_{\min}(\mathbf{C}^H \mathbf{C})} / K} < +\infty. \quad (68)$$

Next, to prove part (ii), it can be seen that  $\lambda_{\min}(\mathbf{C}^H \mathbf{C}) = 0$  if  $\operatorname{Rank}([\mathbf{g}_1, \dots, \mathbf{g}_K]) \neq K$ . Putting this result and  $\phi = 0$  into (43), we obtain  $L_{\Xi}(0) = +\infty$ . On the other hand, if  $\phi > 0$ , we must have  $\sqrt{\phi^2 + \|\mathbf{Cb}\|_2^2} > 0$  due to  $\|\mathbf{Cb}\|_2^2 \geq 0$ . Putting this result into (43), we obtain  $L_{\Xi}(\phi) < +\infty$  if  $\phi > 0$ .

Finally, to prove part (iii) of this theorem, we need the following lemma.

**Lemma 5.**  $\Xi(\mathbf{b})$  is bounded as  $\Phi(\mathbf{b}) \leq \Xi(\mathbf{b}) \leq \Phi(\mathbf{b}) + 2\sqrt{\beta} \phi$ .

*Proof.* To prove the left inequality, notice that  $\|\mathbf{C}\mathbf{b}\|_2 \leq \sqrt{\phi^2 + \|\mathbf{C}\mathbf{b}\|_2^2}$ . Putting this result into  $\Xi(\mathbf{b})$  in (41), we immediately obtain  $\Phi(\mathbf{b}) \leq \Xi(\mathbf{b})$ . On the other hand, to prove the right inequality, we first compute

$$\Xi(\mathbf{b}) - \Phi(\mathbf{b}) = 2\sqrt{\beta} \left( \sqrt{\phi^2 + \|\mathbf{C}\mathbf{b}\|_2^2} - \sqrt{\|\mathbf{C}\mathbf{b}\|_2^2} \right). \quad (69)$$

Then applying the identity  $\sqrt{\phi^2 + x} - \sqrt{x} = \frac{\phi^2}{\sqrt{\phi^2 + x} + \sqrt{x}} \leq \phi$ , where the inequality is due to the monotonic decreasing feature of  $\phi^2/(\sqrt{\phi^2 + x} + \sqrt{x})$  with respect to  $x$ , the right hand side of (69) is upper bounded as

$$2\sqrt{\beta} \left( \sqrt{\phi^2 + \|\mathbf{C}\mathbf{b}\|_2^2} - \sqrt{\|\mathbf{C}\mathbf{b}\|_2^2} \right) \leq 2\sqrt{\beta} \phi. \quad (70)$$

Putting this result into (69), we have  $\Xi(\mathbf{b}) - \Phi(\mathbf{b}) \leq 2\sqrt{\beta} \phi$ . ■

Now, if an  $\epsilon$ -optimal solution  $\mathbf{b}' \in \Delta$  to  $\mathcal{Q}_2$  is obtained with  $\Xi(\mathbf{b}') - \Xi(\mathbf{b}^\diamond) \leq \epsilon$ , then we must have

$$\Phi(\mathbf{b}') \leq \Xi(\mathbf{b}^\diamond) + \epsilon, \quad (71)$$

due to  $\Phi(\mathbf{b}) \leq \Xi(\mathbf{b})$  from the first inequality of Lemma 5. On the other hand, taking the minimum on both sides of the second inequality of Lemma 5, we have

$$\min_{\mathbf{b} \in \Delta} \Xi(\mathbf{b}) \leq \min_{\mathbf{b} \in \Delta} \Phi(\mathbf{b}) + 2\sqrt{\beta} \phi. \quad (72)$$

Putting  $\min_{\mathbf{b} \in \Delta} \Xi(\mathbf{b}) = \Xi(\mathbf{b}^\diamond)$  and  $\min_{\mathbf{b} \in \Delta} \Phi(\mathbf{b}) = \Phi(\mathbf{b}^*)$  into (72), (72) becomes  $\Xi(\mathbf{b}^\diamond) \leq \Phi(\mathbf{b}^*) + 2\sqrt{\beta} \phi$ . Combining this result with (71) leads to  $\Phi(\mathbf{b}') \leq \Phi(\mathbf{b}^*) + 2\sqrt{\beta} \phi + \epsilon$ , and part (iii) of this theorem is proved.

## REFERENCES

- [1] Y. LeCun, Y. Bengio, and G. Hinton, "Deep learning," *Nature*, vol. 521, pp. 436–444, May 2015.
- [2] W. Saad, M. Bennis, and M. Chen, "A vision of 6G wireless systems: Applications, trends, technologies, and open research problems," *IEEE Netw.*, vol. 34, no. 3, pp. 134–142, May/June 2020.
- [3] S. Yu, X. Chen, L. Yang, D. Wu, M. Bennis, and J. Zhang, "Intelligent edge: Leveraging deep imitation learning for mobile edge computation offloading," *IEEE Wireless Commun.* vol. 27, no. 1, pp. 92–99, Feb. 2020.
- [4] S. Wang, Y.-C. Wu, M. Xia, R. Wang, and H. V. Poor, "Machine intelligence at the edge with learning centric power allocation," *IEEE Trans. Wireless Commun.*, vol. 19, no. 11, pp. 7293–7308, Nov. 2020.
- [5] S. Huang, S. Wang, R. Wang, M. Wen, and K. Huang, "Reconfigurable intelligent surface assisted mobile edge computing with heterogeneous learning tasks," *IEEE Trans. Cognitive Commun. Networking*, early access, 2021. DOI: 10.1109/TCCN.2021.3056707.
- [6] Google Research, [Online]. Available: <https://ai.googleblog.com/2017/04/federated-learning-collaborative.html>.



- [7] H. B. McMahan, E. Moore, D. Ramage, S. Hampson, and B. Arcas, "Communication-efficient learning of deep networks from decentralized data," in *Proc. AISTATS*, Fort Lauderdale, Florida, Apr. 2017.
- [8] S. Wang, T. Tuor, T. Salonidis, K. K. Leung, C. Makaya, T. He, and K. Chan, "Adaptive federated learning in resource constrained edge computing systems," *IEEE J. Sel. Areas Commun.*, vol. 37, no. 6, pp. 1205–1221, Jun. 2019.
- [9] M. Chen, Z. Yang, W. Saad, C. Yin, H. V. Poor, and S. Cui, "A joint learning and communications framework for federated learning over wireless networks," *IEEE Trans. Wireless Commun.*, vol. 20, no. 1, pp. 269–283, Jan. 2021.
- [10] T. Zen, O. Semiari, M. Mozaffari, M. Chen, W. Saad, and M. Bennis, "Federated learning in the sky: Joint power allocation and scheduling with UAV swarms," in *Proc. IEEE ICC*, Dublin, Ireland, Jun. 2020.
- [11] Y. Du, S. Yang, and K. Huang, "High-dimensional stochastic gradient quantization for communication-efficient edge learning," *IEEE Trans. Signal Process.*, vol. 68, pp. 2128–2142, Mar. 2020.
- [12] T. T. Vu, D. T. Ngo, N. H. Tran, H. Q. Ngo, M. N. Dao, and R. H. Middleton, "Cell-free massive MIMO for wireless federated learning," *IEEE Trans. Wireless Commun.*, vol. 19, no. 10, pp. 6377–6392, Oct. 2020.
- [13] G. Zhu and K. Huang, "MIMO over-the-air computation for high-mobility multimodal sensing," *IEEE Internet of Things J.*, vol. 6, no. 4, pp. 6089–6103, Aug. 2019.
- [14] M. M. Amiri and D. Gündüz, "Machine learning at the wireless edge: Distributed stochastic gradient descent over-the-air," *IEEE Trans. Signal Process.*, vol. 68, pp. 2155–2169, Mar. 2020.
- [15] G. Zhu, Y. Wang, and K. Huang, "Broadband analog aggregation for low-latency federated edge learning," *IEEE Trans. Wireless Commun.*, vol. 19, no. 1, pp. 491–506, Jan. 2020.
- [16] K. Yang, T. Jiang, Y. Shi, and Z. Ding, "Federated learning via over-the-air computation," *IEEE Trans. Wireless Commun.*, vol. 19, no. 3, pp. 2022–2035, Mar. 2020.
- [17] H. Guo, A. Liu, and V. K. N. Lau, "Analog gradient aggregation for federated learning over wireless networks: Customized design and convergence analysis," *IEEE Internet of Things J.*, early access, 2020. DOI: 10.1109/IIOT.2020.3002925.
- [18] G. Zhu, Y. Du, D. Gündüz, and K. Huang, "One-bit over-the-air aggregation for communication-efficient federated edge learning: Design and convergence analysis," *IEEE Trans. Wireless Commun.*, early access, 2020. DOI: 10.1109/TWC.2020.3039309.
- [19] F. Sotro and W. Yu, "Hybrid digital and analog beamforming design for large-scale antenna arrays," *IEEE J. Sel. Topics Signal Process.*, vol. 10, no. 3, pp. 501–513, Apr. 2016.
- [20] V. Venkateswaran and A. J. van der Veen, "Analog beamforming in MIMO communications with phase shift networks and online channel estimation," *IEEE Trans. Signal Process.*, vol. 58, no. 8, pp. 4131–4143, Aug. 2010.
- [21] Y. Yan, Y. Mao, and B. Li, "SECOND: Sparsely embedded convolutional detection," *Sensors*, vol. 18, no. 10, pp. 3337, Oct. 2018.
- [22] S. Shi, Z. Wang, J. Shi, X. Wang, and H. Li, "From points to parts: 3D object detection from point cloud with part-aware and part-aggregation network," *IEEE Trans. Pattern Anal. Mach. Intell.*, early access, 2020. DOI: 10.1109/TPAMI.2020.2977026.
- [23] R. Gudwin, E. Rohmer, A. Paraense, E. Froes, W. Gibaut, I. Oliveira, S. Rocha, K. Raizer, and A. V. Feljan, "The TROCA Project: An autonomous transportation robot controlled by a cognitive architecture," *Cognitive Systems Research*, vol. 59, pp. 179–197, Jan. 2020.
- [24] A. Dosovitskiy, G. Ros, F. Codevilla, A. Lopez, and V. Koltun, "CARLA: An open urban driving simulator," in *Proc. The 1st Annual Conference on Robot Learning*, 2017, pp. 1–16.
- [25] M. L. Psiaki, S. P. Powell, H. Jung, and P. M. Kintner, "Design and practical implementation of multifrequency RF front ends using direct RF sampling," *IEEE Trans. Microw. Theory Techn.*, vol. 53, no. 10, pp. 3082–3089, Oct. 2005.

- [26] M. P. Friedlander and M. Schmidt, “Hybrid deterministic-stochastic methods for data fitting,” *SIAM J. Sci. Comput.*, vol. 34, no. 3, pp. 1380–1405, May 2012.
- [27] X. Zhang, *Matrix Analysis and Applications*. Beijing, China: Tsinghua Univ. Press, 2004.
- [28] A. Beck, “On the convergence of alternating minimization for convex programming with applications to iteratively reweighted least squares and decomposition schemes,” *SIAM J. Optimiz.*, vol. 25, no. 1, pp. 185–209, 2015.
- [29] Y. Wang, J. Yang, W. Yin, and Y. Zhang, “A new alternating minimization algorithm for total variation image reconstruction,” *SIAM J. Imaging Sciences*, vol. 1, no. 3, pp. 248–272, 2008.
- [30] S. Boyd and L. Vandenbergh, *Convex Optimization*. Cambridge, U.K.: Cambridge Univ. Press, 2004.
- [31] B.-R. Marks, and G.-P. Wright, “A general inner approximation algorithm for nonconvex mathematical programs,” *Operation Research*, vol. 26, no. 4, Jul. 1978.
- [32] A. Ben-Tal and A. Nemirovski, *Lectures on Modern Convex Optimization* (MPS/SIAM Series on Optimizations). Philadelphia, PA, USA: SIAM, 2013.
- [33] S. Wang, L. Cheng, M. Xia, and Y.-C. Wu, “Massive MIMO multicast beamforming via accelerated random coordinate descent,” in *Proc. IEEE ICASSP’19*, Brighton, UK, May 2019, pp. 4494–4498.
- [34] N. Parikh and S. Boyd, “Proximal algorithms,” *Foundations and Trends in Optimization*, vol. 1, no. 3, pp. 127–239, 2014.
- [35] Y. Sun, P. Babu, and D. P. Palomar, “Majorization-minimization algorithms in signal processing, communications, and machine learning,” *IEEE Trans. Signal Process.*, vol. 65, no. 3, pp. 794–816, Feb. 2017.
- [36] M. Sion, “On general minimax theorems,” *Pacific J. Math.*, vol. 8, no. 1, pp. 171–176, 1958.
- [37] Y. Nesterov, “Smooth minimization of non-smooth functions,” *Math. Program.*, vol. 103, no. 1, pp. 127–152, May 2005.
- [38] W. Su, S. Boyd, and E. J. Candes, “A differential equation for modeling Nesterov’s accelerated gradient method: Theory and insights,” *J. Mach. Learn. Res.*, vol. 17, no. 153, pp. 1–43, Sep. 2016.
- [39] A. Beck and M. Teboulle, “A fast iterative shrinkage-thresholding algorithm for linear inverse problems,” *SIAM J. Imaging Sci.*, vol. 2, no. 1, pp. 183–202, Mar. 2009.
- [40] Y. Nesterov, *Introductory Lectures on Convex Optimization: A Basic Course*. Applied Optimization. Springer, 2004.
- [41] L. Condat, “Fast projection onto the simplex and the  $l_1$  ball,” *Math. Program.*, vol. 158, no. 1, pp. 575–585, Jul. 2016.
- [42] T. E. Booth, “Power iteration method for the several largest eigenvalues and eigenfunctions,” *Nucl. Sci. Eng.*, vol. 154, no. 1, pp. 48–62, 2006.
- [43] A. Goldsmith, *Wireless Communications*. Cambridge University Press, 2005.
- [44] L. Deng, “The MNIST database of handwritten digit images for machine learning research,” *IEEE Signal Process. Mag.*, vol. 29, no. 6, pp. 141–142, Nov. 2012.
- [45] A. V. Feljan and Y. Jin, “A simulation framework for validating cellular V2X scenarios,” in *Proc. IEEE IECON*, Washington D.C., Oct. 2018.